Coordination Chemistry Reviews 253 (2009) 754–768

Contents lists available at ScienceDirect

Coordination Chemistry Reviews

journal homepage: www.elsevier.com/locate/ccr

Review

Elucidating enzyme mechanism and intrinsic chemical properties of short-lived intermediates in the catalytic cycles of cysteine dioxygenase and taurine/α-ketoglutarate dioxygenase

Sam P. de Visser*

The Manchester Interdisciplinary Biocenter and the School of Chemical Engineering and Analytical Science, The University of Manchester, 131 Princess Street, Manchester M1 7DN, United Kingdom

Contents

ARTICLE INFO

Article history:
Received 20 February 2008
Accepted 6 May 2008
Available online 14 May 2008

Keywords:
Density functional theory
Enzyme catalysis
Enzyme models
Oxygen activation
Non-heme systems

ABSTRACT

In this review paper theoretical insights obtained through studies of non-heme iron-containing enzymes are discussed. In particular, research on oxygen-utilizing enzymes with a 2-His/1-Asp or 3-His structural motif is the focus of this work with recent examples from studies of cysteine dioxygenase (CDO) and taurine/α-ketoglutarate dioxygenase (TauD) enzymes. Thus, theoretical modeling can be extremely useful in the characterization of short-lived intermediates which either cannot be detected experimentally or have a lifetime that is too short to enable spectroscopic characterization. This paper gives an overview of the knowledge of the catalytic cycles of CDO and TauD with particular emphasis on the processes obtained after dioxygen binding. CDO uses molecular oxygen and transfers both oxygen atoms to cysteine to form cysteine sulfinic acid products. By contrast, in TauD the first oxygen atom of O_2 is donated to α-ketoglutarate to give succinate, carbon dioxide and an oxo–iron active species. The latter is the oxidant that is able to abstract a hydrogen atom from a substrate and rebounds the hydroxyl group to form hydroxylated products. The theoretical (density functional theory (DFT)) studies show that the first step in this dioxygen activation process is the rate-determining step and that the reactions leading to products are highly exothermic as would be expected from an efficient catalytic cycle of an enzyme. Furthermore, theory predicts TauD to be a much more aggressive and efficient catalyst then for instance monoxygenase enzymes such as the cytochromes P450 (P450s). Non-heme enzymes generally react with substrates via single-state reactivity (SSR) patterns on a dominant quintet spin-state surface. Theory has found no evidence of possible alternative oxidants in the reaction mechanisms. The theoretical studies give fundamental insight into processes that proceed too fast to be experimentally studied and give answers to questions regarding the efficiency and nature of the oxidizing species of this fascinating class of enzymes.

* Fax: +44 161 3065201.
E-mail address: sam.devisser@manchester.ac.uk.

0010-8545/$ – see front matter © 2008 Elsevier B.V. All rights reserved.
doi:10.1016/j.ccr.2008.05.001

1. Introduction

Dioxygenase enzymes are important enzymes in nature that utilize molecular oxygen and transfer both oxygen atoms to substrate(s) [1]. By contrast, monoxygenase enzymes also utilize molecular oxygen but transfer only one oxygen atom originating from molecular oxygen to a substrate whereas the other oxygen atom leaves the process as water [2]. Monoxygenase enzymes, such as the cytochromes P450 (P450s) are a versatile group of enzymes involved in important biochemical processes in the body ranging from detoxification of organic substrates in the liver, the biosynthesis of hormones and drug metabolism [3]. The P450s undergo a complicated catalytic cycle where substrate and molecular oxygen bind to the heme center, which triggers a series of events leading to two reduction and two protonation steps and the formation of an oxo–iron species [4]. This oxo–iron species (Compound I, CpdI) in P450 enzymes is the elusive oxidant that never has been detected experimentally, but indirect evidence from product distributions and kinetic isotope effects implicate this oxidant to be the key species that abstracts a hydrogen atom from substrates [5]. Despite the fact that CpdI of P450 is elusive, the oxo–iron active species of other enzymes such as peroxidases has been fully characterized with crystallography, EPR and vibrational spectroscopy [6]. Apart from peroxidases, an oxo–iron active species also has been observed for the non-heme dioxygenase enzyme taurine/α-ketoglutarate dioxygenase (TauD) [7]. This leads to the question, what distinguishes the oxo–iron active species of P450 and TauD enzymes and why is one of these elusive while the other is long-lived? Moreover, why has nature developed two enzymes for essentially similar tasks: the hydroxylation of substrates? Detailed density functional theory (DFT) studies have highlighted the electronic differences and comparisons of heme and non-heme iron catalysts [8,9]. In this review we will give an overview on these and other theoretical studies on dioxygenase enzyme systems and compare the potential catalytic power of dioxygenases with monoxygenases. These theoretical studies are mainly aimed at the 'grey'-zone of the catalytic cycles of enzymes where intermediates are short-lived and cannot be characterized and studied experimentally.

A key property that distinguishes dioxygenase from monoxygenase enzymes is the fact that dioxygenases lack a cofactor. This makes the class of enzymes very suitable for commercial applications especially in comparison to monoxygenases as it will increase their stability and lifetime. Two important dioxygenase enzymes with important functions for human health are TauD and cysteine dioxygenase (CDO), which will be the main focus of this review paper. Both enzymes are involved in the metabolism of cysteine in the body but catalyze different substrate oxidations, see Scheme 1 [10]. Cysteine is a non-essential amino acid that is synthesized in the body from methionine, but is toxic in high concentrations. Therefore, a series of enzymes are involved in the metabolism of cysteine to regulate its concentration in the body. The first step in the metabolism of cysteine is performed by the enzyme cysteine dioxygenase that catalyzes the conversion of cysteine into cysteine sulfinic acid. A subsequent decarboxylation step gives hypotaurine followed by oxygenation to form taurine product. The TauD enzyme catalyzes the hydroxylation of taurine, which thereafter splits off the sulfonate group to give amino-ethanol.

The TauD enzyme is part of the class of α-ketoacid dioxygenases, which is a large class of enzymes with a variety of biochemical functions, such as the synthesis of collagen in mammals, the biosynthesis of antibiotics in bacteria as well as DNA and RNA base repair [11,12]. TauD and CDO both utilize molecular oxygen and incorporate both oxygen atoms into substrate(s), which contrast the behavior of monoxygenase enzymes that use only one atom of molecular oxygen to hydroxylate substrates, while the second oxygen atom leaves the process as water [1,2]. Theoretical studies that focus on short-lived intermediates can give fundamental insight into the electronic and catalytic properties of the catalyst and predict spectroscopic parameters and rate constants for product formation. This knowledge then feeds back into experiment where the predictions and hypothesis are tested and verified. Understanding the catalytic mechanism of these enzymes is important as it may lead to the development of synthetic catalysts for the biosynthesis of fine-chemicals such as drugs [13]. Here we will discuss results of theoretical modeling into the catalytic mechanisms of TauD and CDO enzymes and compare their activity with other non-heme and heme enzymes.

2. The catalytic cycle of cysteine dioxygenase

CDO is an essential enzyme in the human body involved in the metabolism and bioconversion of toxic cysteine [10]. This is a vital process in human health that regulates the cysteine concentration in the body. In cases where the enzyme loses its efficiency this has been correlated to diseases such as Alzheimer's and Parkinson's [14]. Furthermore, a decline in CDO activity has been linked with a neurological disorder associated with iron accumulation [15]. Understanding the catalytic mechanism by which CDO metabolizes cysteine to cysteine sulfinic acid is important for the development of inhibitors and drugs. However, as the catalytic cycle of the enzyme proceeds very fast most intermediates do not accumulate and only limited information regarding its mechanism is known. Surprisingly, only one theoretical study has been reported so far on this enzyme of such importance to human health and only a few experimental studies on intermediates of the catalytic cycle have been reported [16,17]. In particular, experimental work failed to establish a conclusive mechanism after dioxygen binding, therefore, to gain insight into how cysteine is metabolized on an iron center we started our studies on CDO enzymes with establishing the catalytic cycle of the enzyme after dioxygen binding leading eventually to cysteine sulfinic acid products.

CDO is a non-heme enzyme that contains an active center with an iron that is connected to the protein backbone via three histidine bonds of His_{86}, His_{88} and His_{140} (Fig. 1) [16,18]. As follows from the crystal structure the substrate (cysteine) binds as a bidentate ligand via the sulfide and amide groups. The sixth ligand site of iron is reserved for molecular oxygen binding. Studies with isotopically labeled O_2 showed that both oxygen atoms are incorporated into cysteine sulfinic acid products [19]. The second sphere amino acids Tyr_{157}, Cys_{93} and His_{155} have been implicated in stabilizing the reaction process through a tight hydrogen bonding network [16]. Indeed, the carboxylic acid group of substrate cysteine is locked in a salt bridge with the side chain of an arginine amino acid (Arg_{60}), which will fix the substrate in a constraint orientation, presumably

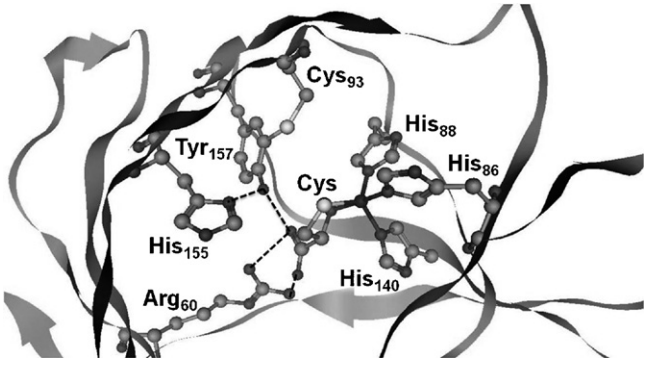

Fig. 1. Extract of the active site of CDO as taken from the 2IC1 pdb.

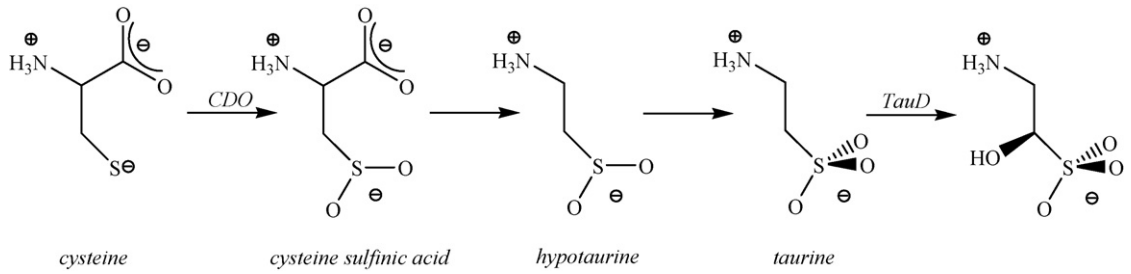

Scheme 1. The metabolism of cysteine in the body and the reaction steps in which CDO and TauD enzymes are involved.

for ideal oxygen abstraction. The carboxylic acid group is further stabilized due to hydrogen bonding of a nearby tyrosinate side chain that in itself is locked in position through an accepting hydrogen bond of His_{155} and a covalent linkage with the side chain of Cys_{93}. This network of hydrogen bonding appears to be important for substrate binding and oxygen transfer mechanisms and also prevents binding of inhibitors.

Recently density functional theory calculations on the catalytic cycle of CDO enzymes have been performed in our group [17]. A large active site model was set-up containing the iron atom with its first and second coordination sphere amino acids that are highlighted in Fig. 1. The four histidine amino acids (His_{86}, His_{88}, His_{140} and His_{155}) were abbreviated to imidazole, as it was shown to be a more faithful mimic of the ligands bound to the oxo–iron species of peroxidases and the TauD enzyme in comparison to imidazolate [20,21]. The side chain of Arg_{60} was abbreviated to methylguanidinium, Tyr_{157} to phenol and its covalently linked Cys_{93} group to methylmercaptane. The starting coordinates from the 2IC1 pdb were used with constraints on one of the atoms of Arg_{60}, His_{155} and Tyr_{157} to keep these amino acids close to their positions in the X-ray structure. Subsequently, molecular oxygen and hydrogen atoms were added to create a model with stoichiometry $FeC_{24}N_{12}H_{37}S_2O_5^+$. Full geometry optimizations were performed for the dioxygen bound complex (**A**) in the quintet spin state and a mechanism was found leading to cysteine sulfinic acid products, see Fig. 2. The dioxygen activation starts with attack of the terminal oxygen atom of the O_2 group in **A** on the sulfur atom of cysteine via a barrier $\mathbf{TS}_A$ of 10.0 kcal mol^{-1} to form a ring-structure (**B**) with an Fe–S–O–O ring. This barrier is the rate-determining step in the catalytic cycle. The ring structure has a considerably weakened O–O bond of 1.513 Å compared to 1.338 Å in ^{5}**A**. This dioxygen bond breaks in the next step of the catalytic cycle to generate cysteine sulfoxide with significant radical character on the substrate. In the subsequent step the sulfoxide group performs an internal rotation to produce structure **D** whereby the oxygen atom has formed a covalent bond with iron and at the same time the sulfur atom is accessible to the other oxygen atom. In the final step of the catalytic cycle the second oxygen atom is transferred to the substrate to generate cysteine sulfinic acid. As can be seen from Fig. 2 the catalytic cycle is exothermic in each step and the lowest barrier is the first one via $\mathbf{TS}_A$. All subsequent barriers are lower in energy than their precursor. Therefore, it will be difficult to experimentally trap and characterize intermediates in the catalytic cycle beyond the dioxygen bound complex. The catalytic cycle devised

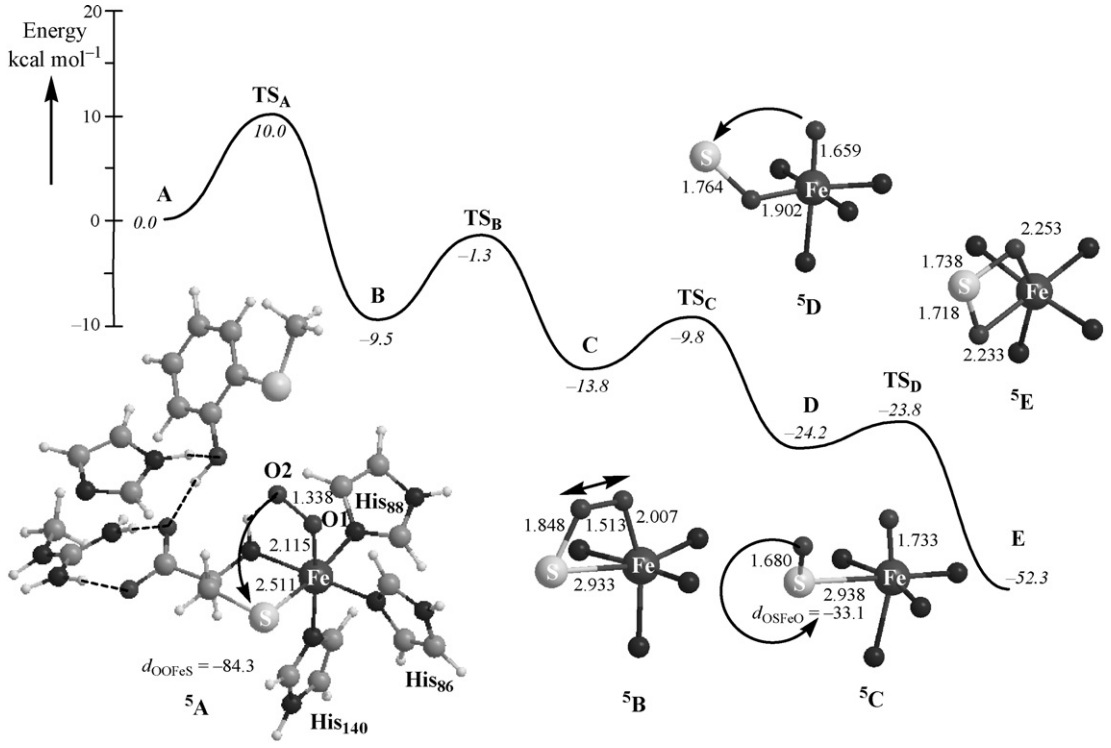

Fig. 2. Catalytic cycle of CDO enzymes starting from the dioxygen bound complex leading to products. All energies are in kcal mol^{-1} relative to the dioxygen bound complex in the quintet spin state (^{5}**A**). Highlights of the optimized geometries of the local minima with bond lengths in Å and dihedral angles (d) in degrees are also shown.

from DFT calculations supports experimental studies, namely both atoms originating from molecular oxygen are incorporated in cysteine sulfinic acid products and no intermediate obtained after dioxygen binding appears to have a lifetime that is long enough to be experimentally detected. Theory also provides new insights such as the formation of a ring-structure, a biradical cysteinyl sulfoxide and an oxo–iron species. In summary, theory predicts most intermediates after dioxygen binding to be short-lived. Dioxygenation of cysteine is a fast process that is efficiently performed by CDO enzymes with a small rate-determining barrier for dioxygen activation.

3. DFT studies on taurine/α-ketoglutarate dioxygenase (TauD)

3.1. Background

CDO enzymes are closely related to the α-ketoacid dioxygenases, such as the α-ketoglutarate dioxygenases (αKGD), which are non-heme enzymes with a common 2-His/1-Asp bound motif [22]. These enzymes are involved in e.g. the biosynthesis of collagen in mammals and antibiotics in microbes [12]. Moreover, the AlkB repair enzymes that also fall into this class of enzymes catalyze the demethylation reaction of methylated DNA and RNA strands [23]. Thus, α-ketoacid dioxygenase enzymes catalyze essential and important biochemical processes.

An extensively studied αKGD enzyme is *E. coli* TauD that contains a non-heme iron with a common 2-His/1-Asp bound motif that utilizes molecular oxygen [11]. The enzyme transfers one oxygen atom from O_2 to α-ketoglutarate (αKG) while the second one is used to hydroxylate taurine. TauD, similarly to CDO enzymes does not require a cofactor, but is able to catalyze oxygenation reactions without external electron donation. Both enzymes contain a non-heme iron center, and in TauD the metal is bound to the protein backbone via linkages of two histidine groups (His_{99} and His_{255}) and one aspartic acid residue (Asp_{101}) via a 2-His/1-Asp motif (Fig. 3) [24,25]. This is a common motif among dioxygenase enzymes and it has been proposed that this motif determines its catalytic properties [26]. As such many synthetic catalysts with a 2-His/1-Asp type motif have been prepared and some indeed show similarities in catalytic properties [1c,27]. In this sense it is surprising that CDO enzymes have a slightly different active site with the metal bound to three histidine groups. In many examples of heme and non-heme catalysis it has been shown that ligands are non-innocent and can actively participate in catalysis so that the 3-His ligand motif in CDO versus the 2-His/1-Asp motif in TauD might lead to catalytic differences [28]. Thus, the heme group was shown to actively participate in arene hydroxylation reactions by shuttling protons [29]. Moreover, in P450 enzymes it was shown that the axial ligand trans to the oxo group in oxo–iron heme environments entices a push-effect that is crucial for the catalytic properties of the heme center [30]. Accordingly, a thiolate anion of a cysteinate residue, as e.g. appears in the cytochrome P450s, induces a push-effect of electrons and thereby makes the oxo–iron group more electronegative, whereas the histidine group in peroxidases pulls electrons away from the active center. As a consequence of this the P450 active center is a monoxygenase oxidant, whereas peroxidases and catalases convert molecular oxygen into peroxides [31].

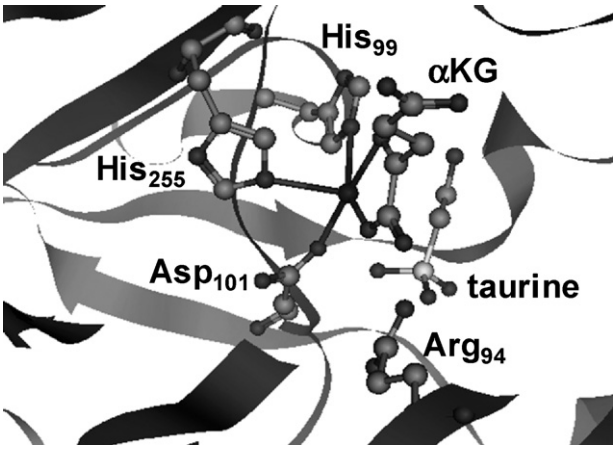

Fig. 3. Extract of the active site of TauD as taken from the 1OS7 pdb with substrates α-ketoglutarate (αKG) and taurine bound in the active site [25].

Fig. 4 shows the catalytic cycle of TauD as based on experimental observations with the important residues highlighted. The cycle starts from the resting state (**F**), where the active center is a six-coordinated iron ligated to two histidine side chains (His_{99}, His_{205}), a carboxylic acid group from Asp_{101} and three water molecules [11a,24]. The initial step in the cycle is binding of αKG, which is a bidentate ligand that displaces two water molecules of the resting state to form complex **G**. This complex has been isolated and found to give an absorption band at 530 nm representing a Fe^{II}-αKG chromophore [32]. The next step in the catalytic cycle is substrate (taurine) binding and although taurine does not bind directly to the iron, its entering into the active site releases the remaining water molecule from the iron complex whereby a five-coordinated complex (**H**) is formed that gives an absorption band at 520 nm [32]. Indeed, magnetic circular dichroism (MCD) studies on the αKG and taurine-binding steps indicated that the system changes from a six-coordinated to a five-coordinated iron system [33]. Upon dioxygen binding (intermediate **I**) the catalytic cycle enters a grey zone, where the intermediates react fast and limited information about the individual intermediates is known. It has been postulated that the dioxygen molecule attacks the αKG group to form ring-structure **J**, followed by decarboxylation to form succinate and an oxo–iron species (complex **K**) [11b,24]. The oxo–iron species subsequently abstracts a hydrogen atom from taurine (complex **L**) and rebounds the hydroxyl group to the rest group to form the product complex (**M**). Release of products (succinate and hydroxylated taurine) and rebinding of water molecules to the active center brings the catalytic cycle back into the resting state. This mechanism has been corroborated with oxygen isotope studies, which revealed that succinate and hydroxylated taurine both carry one oxygen atom originating from molecular oxygen [34]. Stopped-flow experiments on intermediates obtained after dioxygen binding were performed and evidence of at least two stable intermediates was collected [24]. The first stable intermediate is the oxo–iron complex that absorbs at 318 nm and develops after 20–25 ms, but decays after 600 ms. This complex results in the loss of the charge-transfer band of the reactant complex and was identified as containing a quintet spin state with the metal in oxidation state Fe^{IV} [7,35]. Exploratory density functional theoretic calculations on a model system confirmed that the ground state has a quintet spin [35]. Further evidence for the oxo–iron species came from oxygen isotope studies using ^{16}O versus ^{18}O which gave a downshift of the Fe–O frequency by 34 cm^{-1}, whereas typical values for peroxy and hydroperoxo species are 45 cm^{-1} [34]. Hydrogen/deuterium isotope effect studies using taurine and taurine-d_2 proved that this complex is responsible for the hydrogen abstraction step [36]. In the process a second intermediate was identified that occurs after the oxo–iron species and it was assigned as the product complex **M** [37].

Mutation studies of the active site of TauD showed no solvent kinetic isotope effect, which implies that during the catalytic cycle no protons are relayed [38]. Moreover, oxygen binding was found to be the rate-determining step in the catalytic cycle, although it was

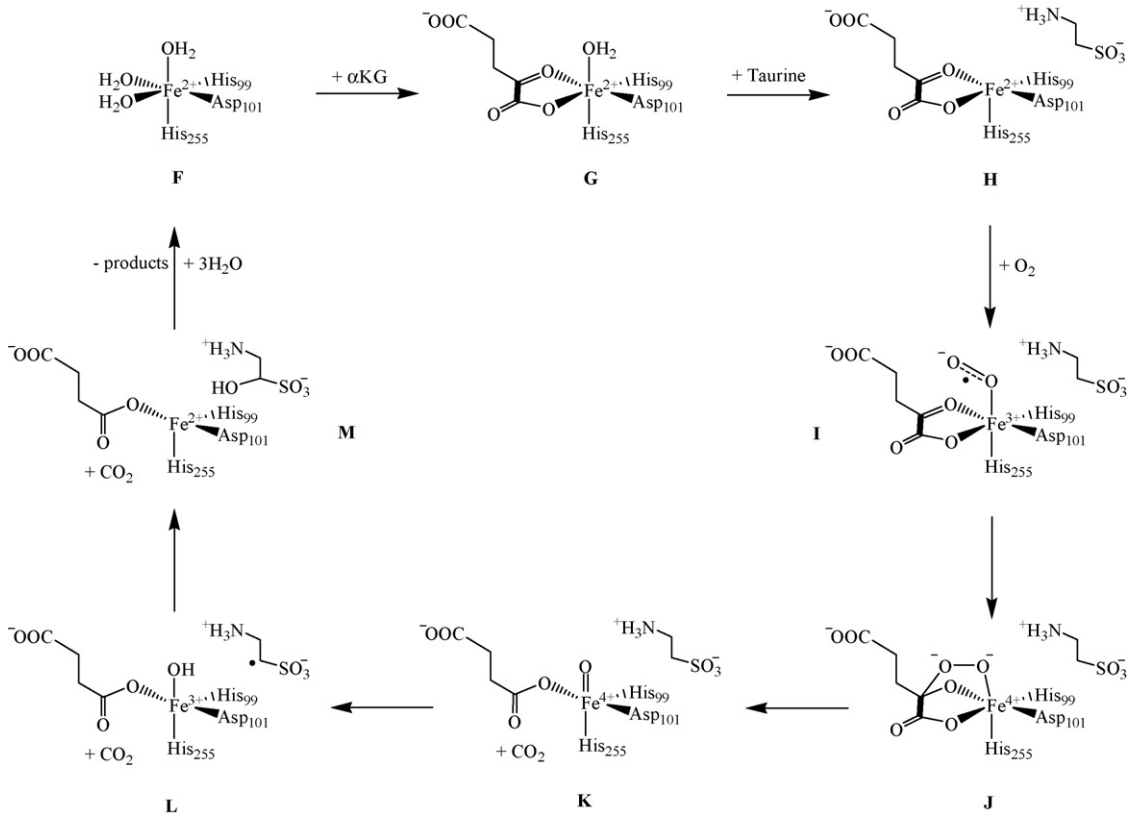

Fig. 4. Catalytic cycle of the TauD enzyme.

acknowledged that the ring structure (**J**, Fig. 4) may have difficult assignable features which cannot be detected. Several crystal structures of intermediates in the catalytic cycle of TauD are available, such as the taurine bound structure (**H**) determined at 1.9 Å resolution and an earlier one at 3.0 Å resolution [25,39]. Upon dioxygen binding no evidence of intermediates except the oxo–iron species is obtained, which means that decarboxylation happens prior to oxo–iron formation. If succinate is added to the enzyme instead of α-ketoglutarate this leads to self-hydroxylation of a tyrosine amino acid or an uncoupling reaction [40].

Despite many experimental studies currently little is known of the process starting with dioxygen binding up to the formation of the oxo–iron species. For the analogous enzyme clavaminic acid synthase (CAS) theoretical studies were reported on the possible intermediates of the catalytic cycle [41]. However, there are some geometric differences between CAS and TauD enzymes which may influence the dioxygen-binding process. Theoretical studies on the catalytic cycle of TauD have been reported [9,41–43] and focused on the following issues: (a) what is the rate-determining step in the dioxygen activation process, (b) are there intermediates with a lifetime that is long-enough to be trapped experimentally, (c) can theory make predictions of spectroscopic features that characterize these short-lived structures, and (d) what is the active oxidant that performs catalysis? In the next few sections answers to these questions will be discussed.

3.2. The catalytic cycle of TauD

Although theoretical calculations on the catalytic cycle of TauD have been reported in several works [41–43], we will follow the cycle described in Ref. [42] in detail as it essentially follows the mechanism of Fig. 4 where a dioxygen bound species (similar to structure **I** in Fig. 4) leads via a bicyclic ring-structure into an oxo–iron active species. The studies in Refs. [41,43] did not incorporate a stepwise mechanism via ring-structure **J** but a synchronous decarboxylation step from the dioxygen bound species. Detailed geometry scans [42], however, showed a local minimum for a bicyclic ring structure, so are more in line with the experimentally proposed mechanism. Therefore we will focus on the mechanism presented in Ref. [42]. Nevertheless, as will be shown below the bicyclic dioxygen complex is a short-lived intermediate and does not play a crucial step in the reaction mechanism. Furthermore, all theoretical studies essentially lead to the same conclusions regarding the catalytic cycle although slightly different methods and models were used.

In TauD the iron is bound to the protein environment via linkages with two histidine and one aspartate group via a typical 2-His/1-Asp motif (see Fig. 3) that appears in many non-heme enzyme systems [1]. Usually in theoretical modeling this motif is abbreviated by imidazole groups for the histidine side chains and acetate for the aspartate side chain [9,44]. Similarly, all studies used α-ketopropionate for αKG with the purpose of keeping the overall charge of the system neutral. In order to obtain accurate energies for the potential energy profile, the number of atoms during the reaction process is retained and as a consequence only the catalytic cycle mechanism is studied starting from the dioxygen bound complex (**1**) until the formation of the oxo–iron species (**4**). Fig. 5 shows the basic reaction mechanism for dioxygen activation on the active center of TauD as identified by these calculations. The mechanism shown in Fig. 5 follows a multistate reactivity pattern [45] on competing spin-state surfaces. The general reaction mechanism is similar to that presented in Refs. [41,43] although the models studied in Ref. [41] also contained two secondary sphere amino acid groups, e.g. an arginine and tyrosine side chain, which

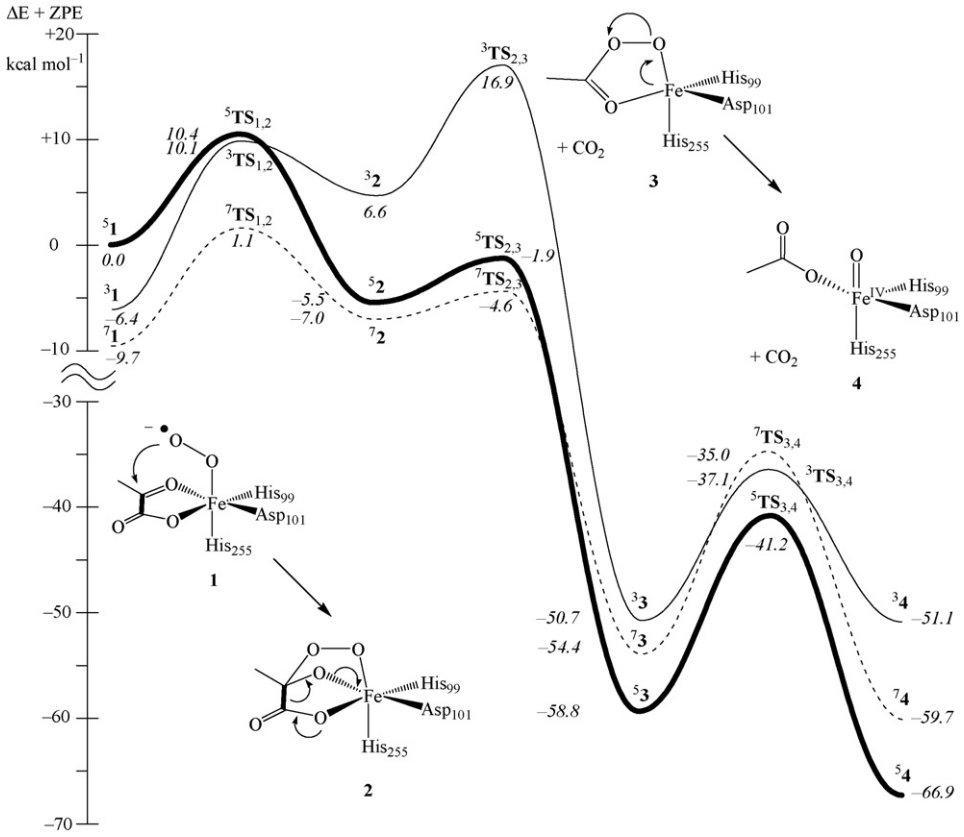

Fig. 5. Potential energy surface for the oxygen activation of the TauD enzyme on the triplet, quintet and septet spin-state surfaces. All energies are obtained at UB3LYP/LACV3P+* level of theory with ZPE corrections using an LACVP basis set, are reported in kcal mol^{-1} and calculated relative to ^{5}**1**.

are missing in the studies of Ref. [42]. However, detailed quantum chemical/molecular mechanics (QM/MM) studies showed that second sphere amino acids as well as the rest of the protein surrounding in this particular system have little effect on the spin-state ordering and relative energies of the oxo–iron intermediate [21]. Therefore, the differences obtained are not due to the choice of the model but more likely the result of basis set and the way zero-point energy and entropy contributions are evaluated.

Let us start with summarizing the complete dioxygen activation mechanism of the TauD model as described in Ref. [42]. The reaction starts from the dioxygen bound complex (**1**) with attack of the terminal oxygen atom in **1** on the α-keto carbon atom of αKG to form a ring-structure (**2**) via a barrier **TS**$_{1,2}$. In a subsequent decarboxylation step, the ring-structure splits off carbon dioxide via a barrier **TS**$_{2,3}$ to form the peroxo acid–iron complex (**3**). The peroxo-bond in the peroxo acid–iron complex thereafter breaks via a barrier **TS**$_{3,4}$ and a carboxylic acid (succinate) and the oxo–iron species (**4**) are formed. As is the case in most transition metal complexes, the systems appear in many close lying spin states, therefore the complete potential energy surface is described in Fig. 5 on the quintet, triplet and septet spin states as identified with a superscript next to the label of the structure.

The potential energy surface for the dioxygen activation of a model of the active center of TauD on the lowest lying triplet, quintet and septet spin states are shown in Fig. 5 [42]. These studies identified two stable intermediates in between the dioxygen bound complex (**1**) and the oxo–iron species (**4**) with a finite lifetime, namely a bicyclic ring-structure (**2**) and a peroxo acid-complex (**3**). As can be seen, initially the septet spin state is the lowest lying, with the triplet and quintet spin states higher by 3.3 and 9.7 kcal mol^{-1}, respectively. At the free energy level the triplet and quintet spin states are higher in energy by 4.2 and 12.7 kcal mol^{-1}. By contrast, Siegbahn et al. find the triplet spin state to be the ground state with the septet and quintet states ΔG = 2.2 and 5.7 kcal mol^{-1} higher in energy. It appears, therefore, that small differences in molecular geometry and choice of the model change the ordering and relative energies of the various spin states of the dioxygen bound complex. Dioxygen binding studies of isopenicillin *N* synthase (INS) showed that small gas-phase models cannot predict the correct spin-state ordering of this complex and full quantum mechanics/molecular mechanics (QM/MM) studies are necessary to predict the correct ground state [46]. Similarly, in the case of TauD to resolve the correct spin-state ordering of the dioxygen bound species a full QM/MM study will be required. By contrast, QM/MM studies on the oxo–iron species of TauD showed little effect of the protein surrounding on the spin-state ordering and relative energies (see Section 3.4) [21]. It appears, therefore, that each intermediate in the catalytic cycle of TauD is influenced differently by the protein environment. Despite this, all model studies on TauD show that the dominant reaction mechanism takes place on the quintet spin-state surface and none of the other spin states play a role of importance in the rest of the mechanism [41,42].

The spin-state ordering of the dioxygen bound species in Fig. 5 is very similar to the one observed for the dioxygen bound species of CDO enzymes [17], which indicates that replacement of the carboxylic acid group in TauD with a histidine group in CDO does not affect spin-state ordering and oxygen binding. However, dioxygen activation to form the ring-structure (**2**) considerably stabilizes the quintet spin state, which comes within 1.5 kcal mol^{-1} of ^{7}**2** and is now well separated from ^{3}**2**. As a matter of fact, on the triplet and septet spin states the initial reaction step, i.e. from **1** to **2**, is endothermic whereas the process is exothermic on the quin-

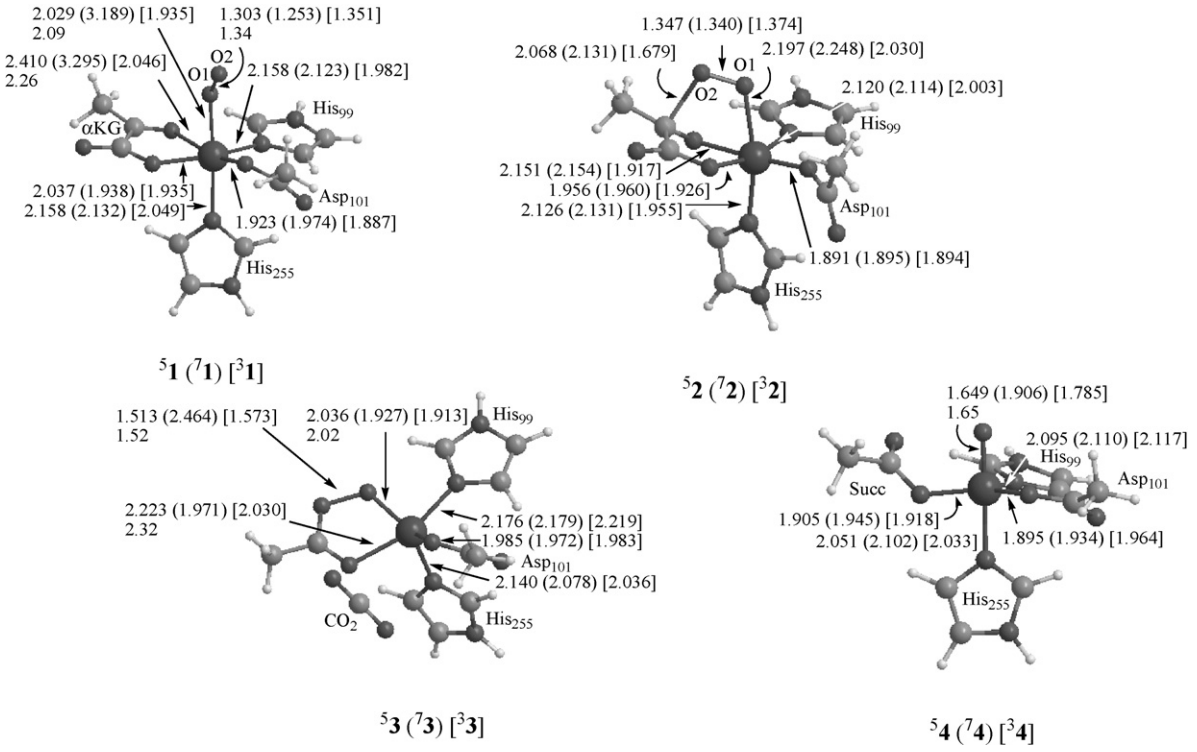

Fig. 6. Optimized geometries of the local minima on the quintet (septet) [triplet] spin surfaces of **1**–**4**. First row data are from Ref. [42] and the second row data from Ref. [41b]. All bond lengths are in Å and the labels of the amino acids were taken from the 1OS7 pdb.

tet spin-state surface. Therefore, based on the relative energies between **1** and **2** a thermal equilibrium between the two structures may be expected.

Only a small barrier ($\mathbf{TS}_{2,3}$) of 3.6 (quintet) and 2.4 (septet) kcal mol^{-1} is required to break the ring-structure (**2**) into carbon dioxide and the peroxo–acid complex (**3**). This implies that the ring-structures on the quintet and septet spin states will have short lifetimes and almost instantaneously react to form **3**. Especially, since the energy difference between $^{5}\mathbf{TS}_{1,2}$ and $^{5}\mathbf{2}$ is 15.9 kcal mol^{-1}. Interestingly, the subsequent barrier ($^{3}\mathbf{TS}_{2,3}$) on the triplet spin-state surface is much higher than the oxygen activation barrier (via $^{3}\mathbf{TS}_{1,2}$) and is 10.3 kcal mol^{-1} above $^{3}\mathbf{2}$, which implies that the triplet reaction will be an energetically difficult process. Moreover, on the triplet surface $^{3}\mathbf{TS}_{2,3}$ is the rate-determining step, whereas the initial oxygen activation barriers via $^{5,7}\mathbf{TS}_{1,2}$ are the rate-determining steps on the high-spin surfaces. Carbon dioxide release (via $\mathbf{TS}_{2,3}$) is an irreversible process whereby the system gains more than 50 kcal mol^{-1} of energy to form the peroxo–acid complex (**3**). This huge exothermicity was not obtained in any of the catalytic steps of CDO enzyme (see Fig. 2) [17], which appears to be a more subtle reaction process where each individual step is accomplished with a small exothermicity. The decarboxylation step in TauD releases a large amount of energy that is necessary to break the peroxide bond to form the oxo–iron active species. This oxo–iron active species of TauD is highly reactive and able to break the aliphatic C–H bond of the substrate and to give hydroxylated products. The peroxosuccinate complex splits into the oxo–iron and carboxylic acid products via a barrier $^{5}\mathbf{TS}_{3,4}$ that is 17.6 kcal mol^{-1} above the energy of $^{5}\mathbf{3}$. The most stable structure on each spin-state surface in Fig. 5 is the oxo–iron species ($^{3,5,7}\mathbf{4}$). Indeed, the oxo–iron complex was trapped and characterized experimentally [7,11b,24,34]. The relatively large O–O bond

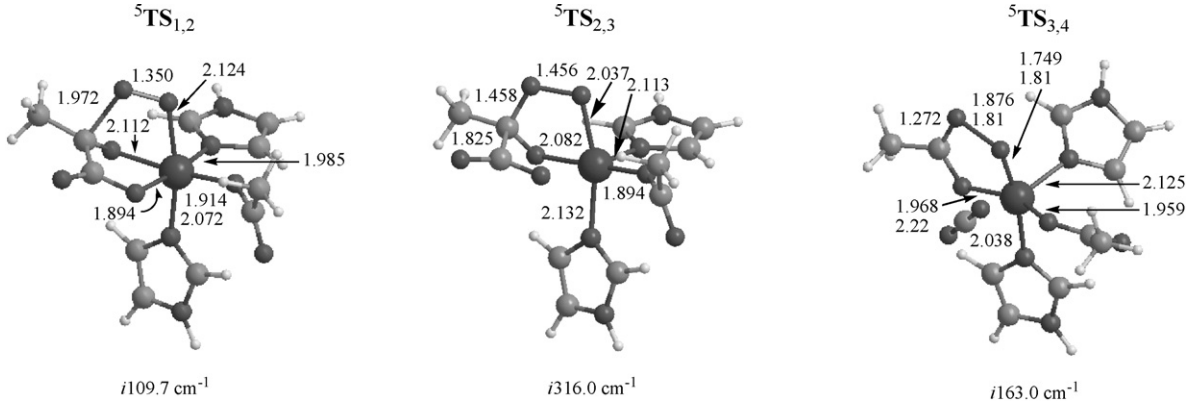

Fig. 7. Optimized geometries of the transition states in the quintet spin state as obtained with Jaguar at UB3LYP/LACVP. First row data are from Ref. [42] and the second row data from Ref. [41b]. All bond lengths are in Å and the imaginary frequency is in cm^{-1}.

breaking barrier (^{5}**TS**$_{3,4}$) indicates that ^{5}**3** may have a relatively long lifetime, which may be long enough to detect and trap it experimentally. In the next section we will discuss its spectroscopic properties and how it can be distinguished from other oxygen binding intermediates in the catalytic cycle. Moreover, structures ^{5}**3** and ^{5}**4** are close in energy and breaking of the O–O bond leads to only a small extra stabilization. As reasoned before [9], the oxo–iron species appears in a quintet spin ground state with the triplet and septet spin states well higher. As a result, the oxo–iron species will react with substrates via single-state reactivity (SSR) on a dominant quintet spin-state surface. This is in contrast to the oxo–iron species in heme-enzymes which contain close-lying quartet and doublet spin states leading to two-state reactivity (TSR) patterns [45] whereby different reaction mechanisms and rate constants are observed on the two spin-state surfaces. Detailed test calculations on the effect of a dielectric constant of $\varepsilon = 5.7$ and 10.65 on the energetics of the reaction mechanism from **1** to **4** were done but most data remained within 1 kcal mol^{-1} from the data of Fig. 5 which indicates that the potential energy profile is not sensitive to an external dipole moment or hydrogen bonding interactions.

Early studies of the catalytic cycle of TauD implicated a septet ground state for the dioxygen bound structure that would lead via a spin state crossing to the quintet spin-state surface prior to oxygen activation [41]. The calculations shown in Fig. 5 indeed support a possible septet/quintet spin state crossing. However, these studies propose the crossing to be somewhat later in the reaction mechanism, namely in or just after the ring structure (**2**). Structures ^{5}**2** and ^{7}**2** have the same electronic configuration with the complete metal 3d block singly occupied together with an unpaired electron in a dioxygen π^* orbital; the latter electron is either antiferromagnetically or ferromagnetically coupled to the metal electrons and as a result these two intermediates are degenerate. The subsequent carbon dioxide release, however, leads to a change in spin-state ordering whereby the quintet spin state is considerably stabilized over the septet spin state. Therefore, the expected septet/quintet spin state crossing will be closely coupled to carbon dioxide release.

Fig. 6 shows the optimized geometries of the critical points along the oxygen activation pathway, whereas Fig. 7 gives the optimized transition states on the quintet spin-state surface. Although, in the gas-phase the ground state of the dioxygen bound and ring-structure species (**1** and **2**) appears to be the septet spin state, close inspection of the geometries show that they have strongly distorted geometries with respect to the X-ray structure [25]. The septet geometries are also completely different from the ones obtained in the triplet and quintet spin states. In particular, in ^{7}**3** and ^{7}**4** the imidazole groups have shifted to the same plane perpendicular to the oxo–iron bond. Since, the septet geometries are very displaced with respect to the X-ray structure the model may not fit the actual enzyme active site anymore and consequently the septet spin mechanism is unlikely in the enzyme and possibly considerably destabilized with respect to the energetics in Fig. 5. In ^{7}**1** the dioxygen moiety is located at a very large distance (3.189 Å) from the iron center, which implies that ^{7}**1** is essentially a triplet dioxygen molecule nearby a quintet iron center. Another interesting feature of this complex is the fact that αKG is not a bidentate ligand but a monodentate ligand since the α-keto group is 3.295 Å away from the iron. By contrast, the optimized structures in the quintet and triplet spin states have the oxygen molecule bound by one atom and the αKG group as bidentate ligand. For completeness we also show optimized geometries from Ref. [41b] in Fig. 6, which show good similarities with the ones from Ref. [42].

Carbon dioxide, once formed quickly dissipates, but stays in the vicinity of the complex (at ≈3.2 Å). Conversion of αKG into succinate (Succ) and CO_2 gives the system a tremendous amount of energy, more than 50 kcal mol^{-1} in the quintet spin state. This is as expected since αKG acts as a cofactor for the reaction process and should give the system sufficient energy so that it is able to perform hydroxylation reactions. Therefore, the dissociation of carbon dioxide from the ring-structure is an irreversible process.

The DFT calculations on the catalytic cycle of TauD are in good agreement with the experimental proposed mechanisms [3] and also with theoretical studies on the dioxygen activation in INS [46]. The latter studies differ from the TauD ones, since the active site of INS contains residues that form hydrogen bonds with the oxygen moiety. Although, these studies used a somewhat larger model for geometry optimizations they were done with several constraints on the geometries. Moreover, the entropic corrections to the energy were based on small models, whereby histidine was abbreviated to ammonia and aspartate by formic acid. Therefore, the spin-state ordering and reaction energies differs somewhat from the ones from Ref. [42]. Nevertheless, the overall reaction barrier on the quintet spin surface leading to decarboxylation is 10.4 kcal mol^{-1}, identical to the one obtained in Ref. [41].

Dioxygen binding to the iron center gives access to several close-lying spin states, namely in the case the spins of the unpaired electrons on the oxygen moiety are aligned with the four unpaired spins on iron. Thus, dioxygen binding gives a ferric–superoxo complex (Fe^{III}–O–$O^{\bullet -}$) in the quintet spin state with orbital occupation: ^{5}**1** : $\pi^*_{x^2-y^2}{}^1\pi^*_{xz}{}^1\pi^*_{yz}{}^1\sigma^*_{xy}{}^1\sigma^*_{z^2}{}^1\pi^*_{OO}{}^1$. The five 3d-type metal orbitals split into a set of 3 t_{2g} and 2 e_g orbitals of which the t_{2g} set are of π^* type (labeled as $\pi^*_{x^2-y^2}$, π^*_{xz} and π^*_{yz}) and the e_g ones of σ^* type (σ^*_{xy} and $\sigma^*_{z^2}$). This complete block of orbitals is singly occupied in the quintet spin state and is antiferromagnetically coupled to an unpaired electron on the dioxygen moiety (π^*). Subsequent oxygen activation of αKG and the generation of the ring-structure (**2**) retain this orbital occupation, but the radical on the ligand weakens the C–C bond enticing carbon dioxide release. Indeed a small barrier leads to the conversion of αKG into peroxo acid (**3**) and CO_2. This process involves the simultaneous electron donation of the metal to the peroxo acid ligand and gives an orbital occupation $\pi^*_{x^2-y^2}{}^1\pi^*_{xz}{}^1\pi^*_{yz}{}^1\sigma^*_{z^2}{}^1$ for ^{5}**3**.

The potential energy surface as shown in Fig. 5 predicts that there are at least two stable intermediates separating dioxygen binding and the formation of the oxo–iron complex, namely the ring-structure (**2**) and the peroxo–acid structure (**3**). The former one is separated by a small barrier leading to the peroxo–acid structure that is also significantly stabilized in energy. Therefore, we do not expect the ring-structure to have sufficiently long lifetime to be detected experimentally. The peroxo–acid structure (^{5}**3**) in its turn is separated by a reasonably large barrier from the oxo–iron complex. Moreover, ^{5}**3** is only 8.1 kcal mol^{-1} less stable than ^{5}**4**. Therefore, ^{5}**3** may very well have sufficiently long lifetime to be detected experimentally.

3.3. Spectroscopic predictions

In order to find spectroscopically identifiable features of intermediates in the catalytic cycle of TauD we investigated the calculated absorption spectra of $^{16}O_2$ and $^{18}O_2$ containing spectra of intermediates **1**, **2**, **3** and **4** [47]. Hausinger and co-workers [34] recently published the $^{16}O_2/^{18}O_2$ difference spectrum of the oxo–iron species (**4**) in the catalytic cycle of TauD and located characteristic frequencies at 583, 821 and 859 cm^{-1} for $^{16}O_2$. The Fe–O stretch vibration was predicted to be at 821 cm^{-1} and downshifts by 34 cm^{-1} after isotopic substitution of $^{16}O_2$ with $^{18}O_2$. We calibrated our calculated absorption spectrum against this Fe–O frequency of Hausinger and co-workers by scaling all vibrations with a factor of 0.9257. A total of seven bands that contain oxygen vibrational modes have been identified for the oxo–iron species in the range from 200 to 900 cm^{-1} (Fig. 8). The lowest three vibrational frequen-

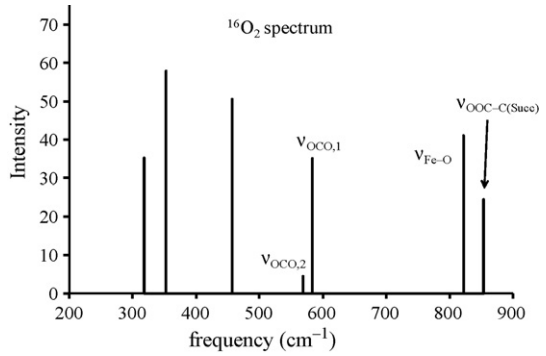

Fig. 8. Vibrational spectrum of oxygen-containing frequencies of the oxo–iron species (^{5}**4**). All frequencies scaled with a factor of 0.9257.

Table 1
Calculated vibrational frequencies of catalytic cycle intermediates and their frequency shifts due to $^{18}O_2$ substitution

Species	Frequency	^{16}O–^{16}O[a]	$^{18}O_2$ shift[a,b]
1	ν_{O-O}	979	−48
2	ν_{O-O}	1027	−61
3	$\nu_{FeOO,bend}$	379	−11
3	$\nu_{OFeO,bend}$	439	−15
3	ν_{O-O}	770	−40
3	$\nu_{C-C,Succ}$	877	−27
4	$\nu_{OCO,2}$	568	−6
4	$\nu_{OCO,1}$	583	−6
4	ν_{Fe-O}	821	−35
4	$\nu_{OOC-C,Succ}$	853	−11

[a] In cm^{-1}; all frequencies scaled with 0.9257.
[b] Difference between $^{16}O_2$ and $^{18}O_2$ vibrational frequencies.

cies in Fig. 8 are bending vibrations in the iron–succinate groups. The frequency located at 853 cm^{-1} represents the C–C stretch vibration of the OOC–CH_3 group of the succinate residue, which is close to a peak in the spectrum of Hausinger and co-workers at 859 cm^{-1}. The calculations predict two carboxylate bending vibrations in the succinate group at 568 cm^{-1} (out-of-plane) and 583 cm^{-1} (in-plane). These three bands together with the ν_{Fe-O} frequency shift after isotopic substitution of oxygen with a heavier isotope and give the system its characteristic $^{16}O_2/^{18}O_2$ difference spectrum, which is in perfect agreement with the experimentally obtained one from Ref. [34]. The experimental difference spectrum obtained by Hausinger and co-workers [34] identified oxygen sensitive vibrations at 583, 821 and 859 cm^{-1} but failed to identify whether those bands were from the oxo–iron species or from another structure in the reaction mixture. Our DFT studies clearly show that all three bands are due to the oxo–iron species and characterize the vibrational modes of these individual bands as arising from the oxo–iron and succinate groups. The calculations, however, provide additional information that cannot be obtained from the experiment, such as the characterization of the frequencies and their individual shifts due to isotopic substitution of O_2.

Subsequently, we calculated the vibrational spectra of $^{16}O_2$ and $^{18}O_2$ containing intermediates **1**, **2** and **3** and the results are shown in Table 1. The dioxygen bound species (**1**) only has one vibration that is influenced by isotopic substitution and is located at 979 cm^{-1}. Also the ring-structure (**2**) has a single dioxygen frequency but it is at a significantly higher value of 1027 cm^{-1}. The strongest vibrational shift observed for the peroxosuccinate complex (**3**) is for the O–O stretch vibration in the peroxo group, which drops from 831 to 789 cm^{-1} (−42 cm^{-1}). The calculations, however, predict this vibration to have quite small intensity, so it may be difficult to experimentally identify this vibration. Similarly, to the oxo–iron complex discussed above the C–C stretch vibration in the peroxosuccinate is downshifted significantly from 947 to 918 cm^{-1} (−29 cm^{-1}). In the oxo–iron species all bending vibrations in which the two ^{18}O atoms are involved are located in between 300 and 650 cm^{-1} and showed little change after isotopic substitution. By contrast, in the peroxosuccinate complex a considerable change in the OFeOO bending vibration is found, which drops from 474 to 458 cm^{-1} (−16 cm^{-1}). Another bending vibration drops by 11 cm^{-1} from 409 cm^{-1}. In summary, the peroxosuccinate system has a unique O–O stretch vibration that shifts from 831 to 789 cm^{-1} after isotopic substitution. Moreover, in comparison to the oxo–iron species the Fe–O stretch vibration is missing and significant larger isotopic shifts for the bending vibrations (474 and 409 cm^{-1}) are observed. Therefore, isotopic substitution of molecular oxygen should give a characteristic absorption spectrum of each intermediate (**1**, **2**, **3**, and **4**) in the catalytic cycle of TauD with unique $^{16}O_2/^{18}O_2$ shifts that should enable experimental detection

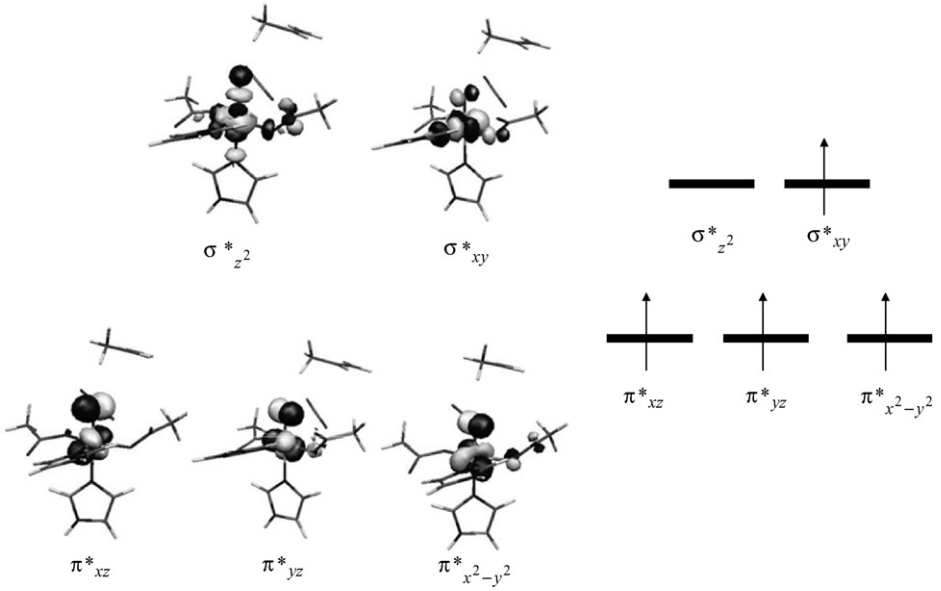

Fig. 9. Molecular orbitals of the oxo–iron species of TauD (left-hand-side) and the orbital occupation in the quintet spin state (right-hand-side).

of intermediates in the catalytic cycle of TauD as well as in other non-heme enzymes and biomimetic model complexes.

3.4. The oxo–iron species of TauD

The hydroxylation reaction mechanism by the oxo–iron active species of TauD requires the transfer of two electrons from the substrate into the iron system. To understand these relevant electron transfer processes, we will start with a description of the high-lying occupied and low-lying virtual orbitals of the oxo–iron species. Fig. 9 shows the high-lying occupied and low-lying virtual orbitals of the oxo–iron complex of TauD. The five orbitals depicted in Fig. 9 all originate from the metal 3d-orbitals and split into a typical 3-below-2 (t_{2g}–e_g) set of orbitals. The three t_{2g} orbitals are of π^* type and reflect the antibonding interactions of the metal 3d-orbitals with 2p-orbitals on the oxo-group, while the e_g set of orbitals are σ^*-type orbitals. These σ^* orbitals are along the *z*-axis (His_{255}–Fe–O) and for the interactions in the *xy*-plane. Mössbauer spectra and DFT calculations predicted the ground state to be a quintet spin state [35].

Because different models and methods of the dioxygen bound species of TauD give differences in spin-state ordering and relative energies, it was decided to do a series of QM/MM calculations on an active site model of TauD. These calculations were compared to the small model complexes and tested the effect of the (protein) environment on the optimized geometries and spin-state ordering of the oxo–iron species. Two computational methodologies were investigated and compared: (a) DFT modeling using the model discussed in the previous section and (b) QM/MM calculations on a large active site region of TauD containing over 650 atoms [9,21]. Model (a) is labeled here as $^5\mathbf{4}_{DFT}$ and model (b) as $^5\mathbf{4}_{QM/MM}$ in the following. Fig. 10 displays optimized geometries of the oxo–iron species of TauD in the quintet spin states as calculated with the QM/MM model of Ref. [21] and compared to the small DFT model of Ref. [42]. The QM region in the QM/MM calculations used apart from the atoms of the small DFT model also the methylguanidinium group of Arg_{270} and taurine substrate. On the left-hand-side, a 3D-drawing is shown that highlights the QM region with tubes while the dashed amino acids in the background are part of the MM region. The QM/MM geometries are close to the ones obtained before using small DFT complexes. The Fe–O bond lengths obtained for the DFT models are 1.649, 1.785 and 1.906 Å for $^5\mathbf{4}$, $^3\mathbf{4}$ and $^7\mathbf{4}$, respectively while with QM/MM methods values of 1.656, 1.781 and 1.949 Å were obtained. Thus, the extra hydrogen bonding interactions of e.g. the protons of Arg_{270} with the oxo and succinate groups within the active site pocket seem to have only little effect on the optimized geometries of the oxo–iron species of TauD. Therefore, inclusion of second sphere amino acids, as done in the work of Ref. [41], does not change the spin state ordering. Moreover, perturbations due to the protein environment do not seem to affect the optimized geometries of the active species of TauD.

The Fe–O distance of TauD is typical for oxo–iron complexes and matches the experimentally obtained distances of the oxo–iron species of horseradish peroxidase (HRP) and catalase excellently [6,48]. DFT calculations on the oxo–iron species of HRP and P450 predicted Fe–O distances of 1.621 and 1.651 Å, respectively, which are values very close to the ones shown here [44a]. The Fe–N_{His} distances of the oxo–iron species of TauD are between 2.05 and 2.10 Å, similarly to the one in HRP [44a].

3.5. Catalytic properties of the oxo–iron species of TauD

TauD is not the only enzyme that possesses an oxo–iron active center that activates aliphatic C–H bonds. In particular, the cytochromes P450 are heme enzymes involved in many biochemical processes ranging from detoxification processes in the liver, drug metabolism and the biosynthesis of hormones [2]. To test the catalytic properties of the oxo–iron active species of TauD and to find out how it compares to the oxo–iron species of heme enzymes such as the cytochromes P450, we ran detailed DFT calculations on models of TauD and P450 and studied the reactivity patterns versus a common substrate (propene). Although propene is not the natural substrate of these enzymes, it will give insight into the relative capabilities of substrate hydroxylation and epoxidation of these two enzymes. Thus, to find out what the fundamental differences in catalytic properties of heme and non-heme oxo–iron oxidants

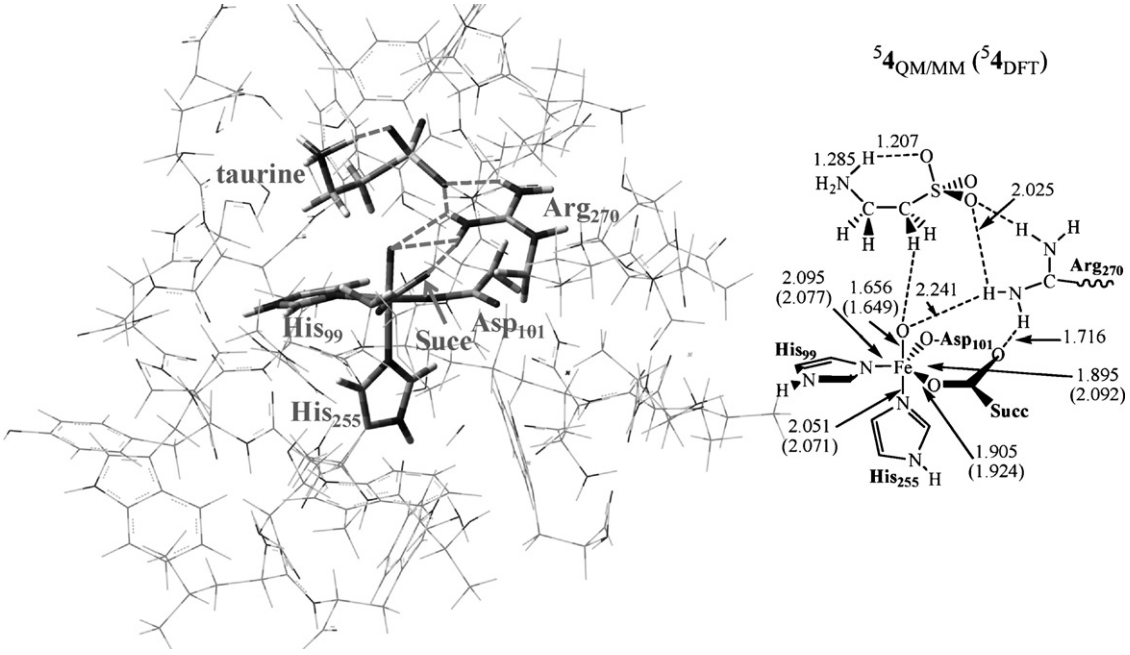

Fig. 10. QM/MM and DFT optimized geometries of the oxo–iron species of TauD with bond lengths in Å [21].

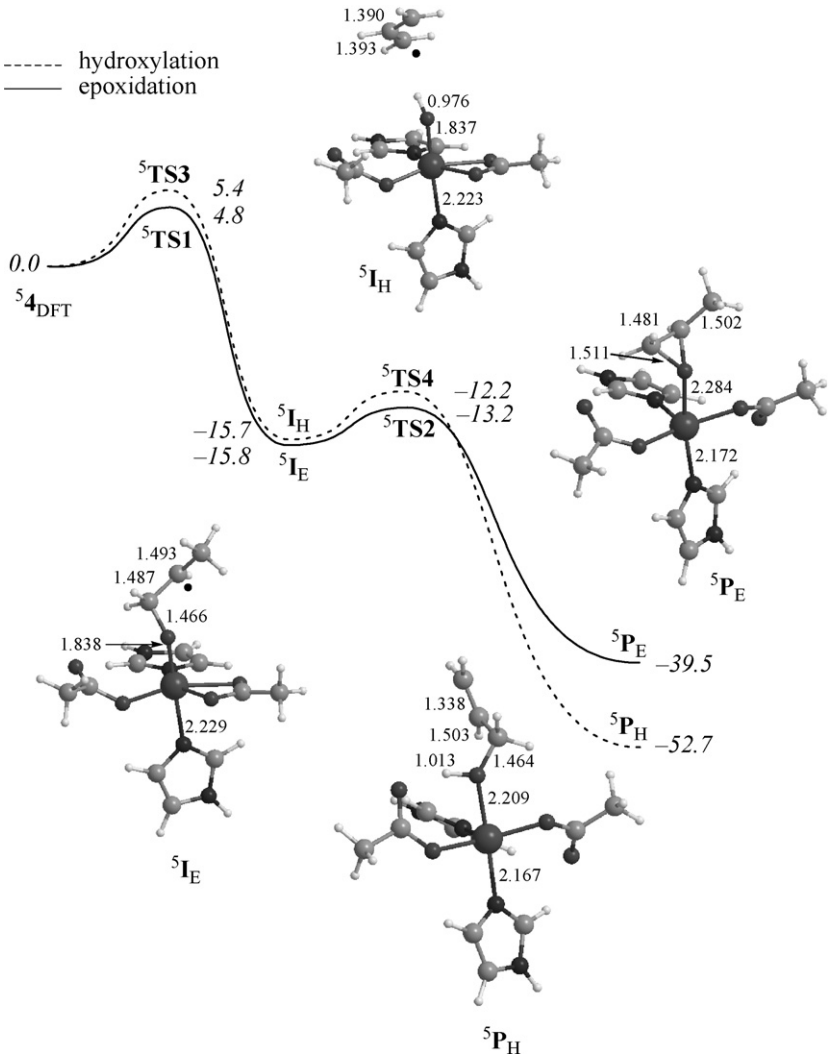

Fig. 11. Reaction profile of the epoxidation and hydroxylation of propene by the oxo–iron species of TauD (^{5}**4**$_{DFT}$) as obtained from UB3LYP/LACVP optimizations in Jaguar [9]. All energies (in kcal mol^{-1}) are at the LACV3P+* level of theory with ZPE corrections included. Also shown are optimized geometries of the local minima with bond lengths in Å.

are, the competitive epoxidation and hydroxylation of propene was studied [9]. Earlier work on this reaction by an oxo–iron model of P450, HRP and some synthetic oxo–iron oxidants versus propene showed that it reacts via multistate reactivity patterns on competing doublet and quartet spin-state surfaces [49]. Moreover, subtle environmental perturbations were shown to influence the regioselectivity of reaction and thereby the product distributions. Fig. 11 shows the potential energy profile of propene epoxidation and methyl group hydroxylation by the oxo–iron species of TauD. The epoxidation reaction mechanism is stepwise via a radical intermediate ($\mathbf{I}_E$) that is separated from reactants via an initial C–O bond activation barrier **TS1** and from epoxide products ($\mathbf{P}_E$) via a ring-closure barrier **TS2**. Due to extra exchange stabilization of the transition state and the intermediate complex in the quintet spin state the rate-determining step is only 4.8 kcal mol^{-1}. The formation of the radical intermediate is an extremely exothermic process by 15.8 kcal mol^{-1} and is separated by a small ring-closure barrier (of 2.6 kcal mol^{-1}) leading to products. We also tested the mechanisms on the lowest lying triplet and septet spin states but found them much higher in energy so that the reaction will take place via single-state reactivity on a dominant quintet spin-state surface. The hydroxylation follows a stepwise mechanism as well with an initial hydrogen abstraction barrier (**TS3**) leading to a hydroxo–iron complex ($\mathbf{I}_H$) that rebounds the hydroxyl group to the substrate via a rebound transition state **TS4** to form propenol product complex ($\mathbf{P}_H$). The hydroxylation barrier is only 5.4 kcal mol^{-1}, which is just 0.6 kcal mol^{-1} higher than the epoxidation barrier, so that it may be assumed that in the gas-phase the two processes will be competitive. The process from $^5\mathbf{I}_H$ to $^5\mathbf{P}_H$ encounters a small rebound barrier of 3.5 kcal mol^{-1}, and therefore the radical intermediate will have sufficient lifetime to undergo rearrangement.

The reaction barriers of 4.8 (**TS1**) and 5.4 (**TS3**) kcal mol^{-1} obtained for propene epoxidation and hydroxylation by the oxo–iron species of TauD are well lower than those calculated for the same reaction with models of HRP and P450 CpdI where barriers (**TS1**) of 8.5 and 12.3 kcal mol^{-1}, respectively were obtained using the same methods and basis sets [49]. These barriers imply that the oxo–iron species of TauD will be a much more efficient oxidant than heme-enzymes and should be able to hydroxylate strong C–H bonds. Our calculations have identified some critical and fundamental differences between heme and non-heme oxo–iron oxidants that may determine these reactivity differences.

The oxygenation reaction of substrates involves a two-electron reduction of iron, which in the epoxidation and hydroxylation mechanisms follow the same electron transfer mechanisms (Fig. 12). The systems starts from an oxo–iron(IV) species with

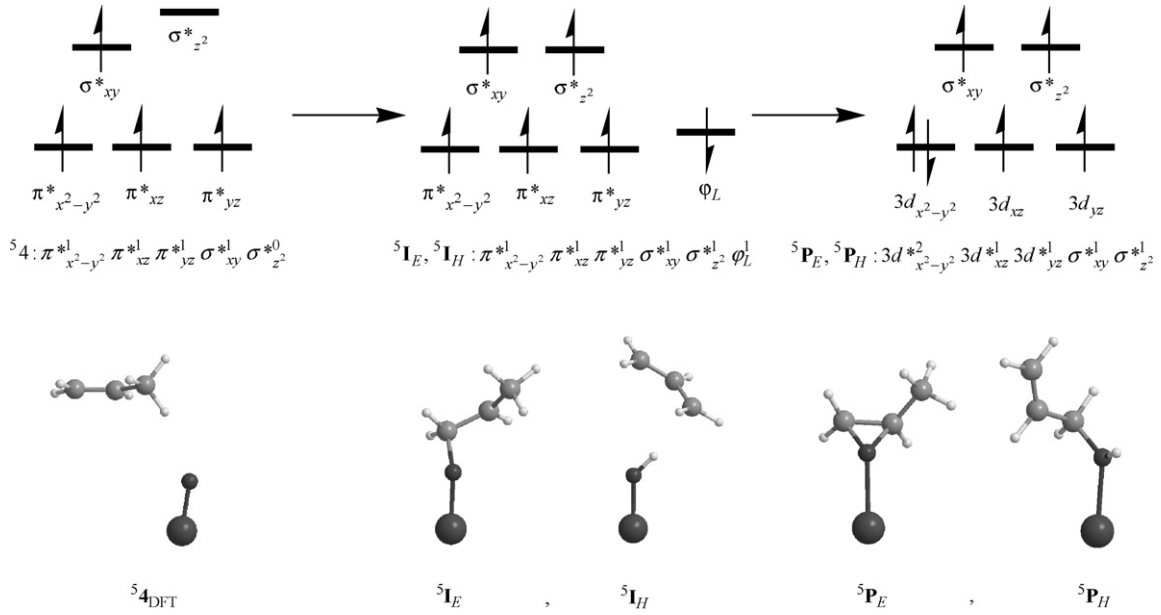

Fig. 12. Orbital occupation of reactants, intermediates and products during the epoxidation and hydroxylation reactions. Below are shown extracts of the relevant structures showing the iron, oxo and propene groups.

four electrons occupying the lowest four metal 3d-orbitals: $\pi^*_{x^2-y^2}$, π^*_{xz}, π^*_{yz}, σ^*_{xy} (Fig. 9). Approach of the substrate leads either to a hydrogen abstraction from the substrate to form the hydroxo–iron complex ($^5\mathbf{I}_H$) or a C–O bond formation gives a radical $^5\mathbf{I}_E$. In both cases this reaction is accomplished by an electron transfer from the substrate into the virtual σ^* orbital to create a fully exchange coupled 3d-system on the metal coupled to a radical (with opposite spin) on the substrate rest-group (in orbital φ_L). This exchange stabilized metal system will lower the energy of the radical intermediate with respect to reactants as indeed observed in the reaction mechanism. In the subsequent radical rebound or ring-closure step via **TS4** or **TS2** a second electron is transferred from the substrate into the iron 3d-system that fills one of the π^* orbitals with a second electron. Due to transfer of the oxygen atom to the substrate the three π^* orbitals become nonbonding orbitals and hence are labeled as $3d_{x^2-y^2}$, $3d_{xy}$ and $3d_{yz}$ in the product complexes. Thus, during the reaction the metal changes oxidation state from Fe^{IV} in reactants to Fe^{III} in intermediates to Fe^{II} in the product complexes.

Non-heme oxidants such as the oxo–iron species of TauD have a different electronic ground state to P450 systems and also show different electron transfer processes during monoxygenation reactions. Thus, the oxo–iron active species of P450 has an electronic ground state with close lying doublet and quartet spin states [50], while the oxo–iron species of TauD has a quintet spin ground state. Furthermore, P450 has an extra oxidation equivalent on the heme (a radical) that can abstract one of the electrons during the monoxygenation process so that the metal only needs to take a single electron and is reduced from Fe^{IV} to Fe^{III} in the reaction process. Due to differences in these electron transfer processes also the approach of the substrate on the catalyst is different. Thus, in TauD the substrate approaches from the top to get ideal orbital overlap with the σ^* orbital, while in P450 the substrate approaches side-ways and an electron is transferred to the heme [51].

Table 2 summarizes the different properties of several heme and non-heme oxidants, such as TauD, P450 and HRP, with respect to monoxygenation of propene as revealed by DFT calculations on model complexes [9,49,51,52]. In Table 2, CpdI-Cl represents a biomimetic oxo–iron porphyrin model with a chloride axial ligand, while Fe=O(TMCS)$^+$ is a non-heme oxo–iron oxidant with a TMCS = 1-mercaptoethyl-4,8,11-trimethyl-1,4,8,11-tetraazacyclotetradecane ligand [51,52a]. Propene hydroxylation and epoxidation by heme enzymes, such as P450, HRP or synthetic biomimetics, takes place on competing doublet and quartet spin-state surfaces via two-state reactivity patterns. However, this is not always the rule as for instance sulfoxidation and arene hydroxylation were shown to appear on one dominant spin-state surface: sulfoxidation on the quartet spin surface and arene hydroxylation on the doublet spin surface [28ab,53] Moreover, it should also be noted that in some cases it was shown that side reactions leading to by-products only are possible on one of the two spin-state surfaces [43c,54]. Examples of these by-products in epoxidation reactions are suicidal complexes and aldehydes [55]. In TauD the quintet spin state is the sole oxidant so all products originate from the same species in the quintet spin state. Interestingly all oxo–iron models catalyze propene epoxidation favorably over hydroxylation by about 0.6–1.2 kcal mol^{-1} in the gas-phase. The only exception to this rule is Fe=O(TMCS)$^+$ where the approach of substrate is sterically hindered by the TMCS ligand, which destabilizes the epoxidation barrier more than the hydroxylation barrier [51].

Table 2
Reactivity differences of different oxo–iron species[a]

	TS1[b]	TS3[b]	SSR/TSR[c]	Heme	Reference
TauD	4.8	5.4	SSR	No	[9]
Fe=O(TMCS)$^+$[d]	17.9	15.0	SSR	No	[51]
HRP	9.7 (8.5)	10.9 (9.7)	TSR	Yes	[49c]
Catalase	10.3 (9.7)	12.0 (11.3)	TSR	Yes	[52b]
CpdI-Cl	12.7 (11.7)	14.8 (12.9)	TSR	Yes	[52a]
P450	12.8 (12.3)	14.0 (13.0)	TSR	Yes	[49b]
CpdI(ImH(P))[e]	13.6 (12.4)	19.1 (13.0)	TSR	Yes	[52c]

[a] Energies in kcal mol^{-1} obtained at UB3LYP/LACVP with ZPE included at UB3LYP/LACV3P+*.
[b] Low-spin barriers in parenthesis, high-spin barriers out of parenthesis.
[c] Single-state reactivity (SSR) or two-state reactivity (TSR).
[d] Non-heme oxo–iron model with cyclamen ligand.
[e] CpdI(ImH(P)) is a peroxidase mutant with one of its nitrogen atoms replaced by phosphorus.

Recently, trends of hydrogen abstraction bond strengths of oxo–iron oxidants, were explained with a valence bond (VB) model and we applied this also to the oxo–iron species of TauD [9,56,57]. Thus, if we assume that an oxo–iron species reacts with an alkane (Alk–H) by a hydrogen abstraction reaction to form a hydroxo–iron complex and an Alk radical (Eq. (1)), it follows that the reaction energy or enthalpy of Eq. (1) is the energetic difference of the dissociation of the C–H bond (Eq. (2)) and the formation of the FeO–H bond (Eq. (3)). Indeed, experimental studies on hydrogen abstraction mechanisms of non-heme biomimetic oxidants showed that the rate constants of C–H hydrogen abstraction reactions by various oxo–metal systems give a linear correlation with the strength of the C–H bond that is broken in the process. In other words, the reaction exothermicity of the hydrogen abstraction reaction correlates with the bond dissociation energy BDE_{C-H} of the C–H bond of the substrate that is broken as well as to the strength of the newly formed FeO–H bond, Eqs. (2) and (3) [58]. In particular, the studies of Kaizer et al. showed that non-heme oxo–iron complexes are able to hydroxylate alkane C–H bonds with a BDE_{C-H} as high as 99.3 kcal mol^{-1} [59].

$$Fe{=}O + Alk{-}H \rightarrow FeO{-}H + Alk^{\bullet} \quad (1)$$

$$Alk{-}H \rightarrow Alk^{\bullet} + H^{\bullet} + BDE_{C-H} \quad (2)$$

$$FeO{-}H \rightarrow Fe{=}O + H^{\bullet} + BDE_{O-H} \quad (3)$$

The reaction enthalpy (ΔH_r) for the hydrogen abstraction reaction (Eq. (1)) is then essentially the difference in energy between the bond dissociation energy of the broken C–H bond (BDE_{C-H}) and the newly formed O–H bond (BDE_{O-H}):

$$\Delta H_r = BDE_{C-H} - BDE_{O-H} \quad (4)$$

Thus, for a series of reactions with the same substrate but different oxo–iron oxidants the value of BDE_{C-H} is a constant and ΔH_r should correlate linearly with BDE_{O-H}. In the past we studied the catalytic properties of many oxo–iron systems versus a range of substrates. As an example we will compare the ones with propene as a substrate here that has a BDE_{C-H} of 82.6 kcal mol^{-1} [57]. We have studied propene hydroxylation by models of TauD, P450, HRP, CpdI-Cl, catalase, cytochrome *c* peroxidase (CcP) and several inorganic oxidants [9,49,52]. From these studies, we estimated values for BDE_{O-H} of the oxo–iron oxidants and the results are schematically depicted in Fig. 13. Thus, the oxo–iron active species of TauD creates the strongest FeO–H bond with a strength of 98.3 kcal mol^{-1}, while typical heme systems, such as P450, HRP and CpdI-Cl, give much smaller values in the range of 87.4–88.7 kcal mol^{-1}. The FeO–H strength is almost identical to the one obtained for a synthetic oxo–iron oxidant with a polyoxometallate (POM) structure [60]. It may be anticipated, therefore, that POM and heme systems will give

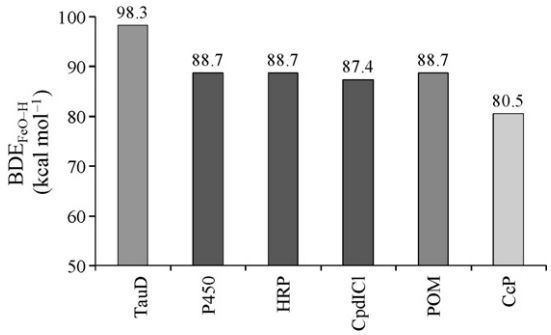

Fig. 13. FeO–H bond dissociation energies (BDE_{O-H}) of several oxo–iron complexes as calculated with DFT UB3LYP/LACV3P+* with ZPE corrections at LACVP level of theory.

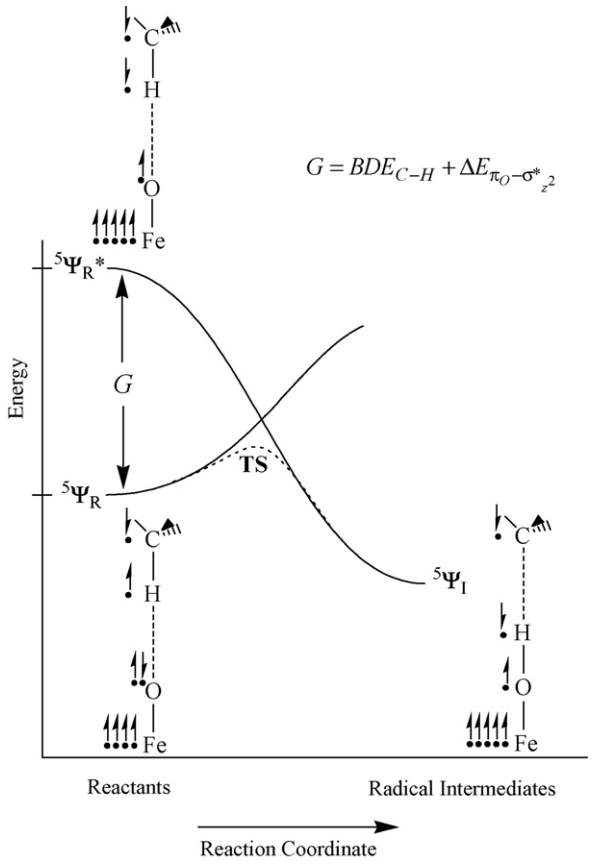

Fig. 14. Valence bond curve crossing diagram for the hydrogen abstraction step from ^{5}**1** to ^{5}**4** in TauD. The electrons next to iron represent the 3d-orbitals as depicted in Fig. 9 and the ones next to oxygen are electron occupying the π_O orbital along the Fe–O bond. Reprinted with permission from Ref. [9b]. Copyright 2006 the American Chemical Society.

similar reaction patterns with substrates. The only heme-system with a much weaker FeO–H bond is the oxo–iron species of CcP, so that it is expected to be a much less efficient oxidant. This is presumably due to the fact that CcP has a protein radical rather than a heme radical and the transfer of the electron will take place over a much larger distance.

In order to establish why TauD has a much larger BDE_{O-H} value than related oxidants, we created a valence bond electron transfer mechanism for the hydrogen abstraction reaction from ^{5}**4** to $^5\mathbf{I}_H$, see Fig. 14 [9]. As shown in Fig. 9 the oxo–iron active species has orbital occupation $\pi^*_{x^2-y^2}{}^1\pi^*_{xz}{}^1\pi^*_{yz}{}^1\sigma^*_{xy}{}^1$, which essentially corresponds to four unpaired electrons on the metal. These four unpaired electrons are identified with a dot next to the iron atom. In addition, the oxo–iron species of TauD also has a lone-pair on the oxygen atom and two electrons in the C–H bond of the substrate that play a role in the reaction mechanism and we have identified these separate electrons in Fig. 14 with a dot and an arrow with the spin direction. The electronic ground state of the oxo–iron species is the reactant state wave function, $^5\Psi_R$. In the hydroxo–iron complex (the radical intermediate) the system is characterized by a $\pi^*_{x^2-y^2}{}^1\pi^*_{xz}{}^1\pi^*_{yz}{}^1\sigma^*_{xy}{}^1\sigma^*_{z^2}{}^1$ configuration on iron, which is identified with five dots next to the metal representing the quintet situation on iron. In addition this complex has a spin-paired couple in the O–H bond and an unpaired electron with β-spin on the carbon atom of the substrate to give the radical intermediate with an overall wavefunction $^5\Psi_I$. This wavefunction extrapolates to $^5\Psi_R$* that represents wavefunction $^5\Psi_I$ in the reactant geometry. Upon intermediate formation the system crosses from wavefunction $^5\Psi_R$

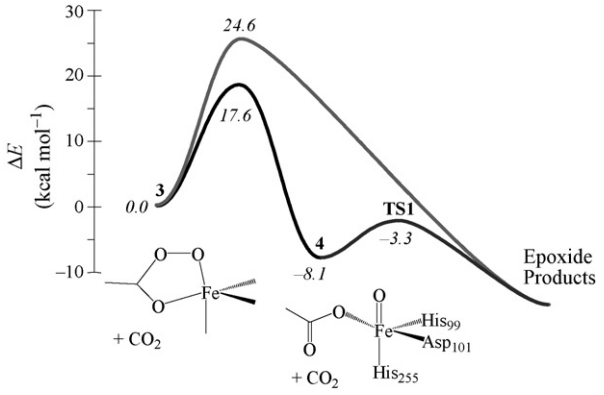

Fig. 15. Potential energy profile for the competitive epoxidation by the peroxosuccinate intermediate (**3**) and the oxo–iron species (**4**) of the TauD enzyme. All energies are obtained at the UB3LYP/LACV3P+* level of theory with ZPE at LACVP level.

to $^5\Psi_I$, thereby giving rise to a transition state for the hydrogen abstraction process. It has been shown that the barrier height for the crossing point (i.e. the transition state) between $^5\Psi_R$ and $^5\Psi_I$ is a fraction (f) of the vertical excitation energy (G) from $^5\Psi_R$ to $^5\Psi_R{}^*$. This excitation energy (G) corresponds to the difference in energy between singlet-paired and triplet-coupled electrons in the C–H bond in the reactant geometry. In addition, G contains a contribution for the excitation energy of an electron from the lone-pair on the oxygen atom (π_O) to the $\sigma^*_{z^2}$ orbital. As the singlet-triplet energy gap for the C–H bond is proportional to BDE_{C-H} it is evident that the excitation energy G and hence the height of the barrier (transition state) will also be proportional to BDE_{C-H} [57,61]. Thus, the barrier height is dependent on the energy level of $^5\Psi_I$, and if this wavefunction can be lowered in energy this should result in lowering of the barrier height of the hydrogen abstraction reaction. The formation of a strong O–H bond in non-heme complexes such as TauD means that the wavefunction $^5\Psi_I$ is low in energy and consequently the hydrogen abstraction reaction is highly exothermic and the reaction barrier is small. As a consequence of this five-coordinated oxo–iron complexes as appear in the TauD enzyme have stronger O–H bonds and react with lower barriers with respect to corresponding heme enzymes. Therefore, there are fundamental differences in reactivity patterns of heme and non-heme oxidants.

3.6. Alternative oxidant hypothesis

As was shown in Fig. 5, the most stable intermediate after dioxygen binding is the oxo–iron species. However, its precursor in the catalytic cycle (the peroxosuccinate complex, **3**) is only 8.1 kcal mol^{-1} less stable and encounters a barrier of 17.6 kcal mol^{-1} for the dioxygen bond breaking to form the oxo–iron species. As a consequence, the peroxosuccinate complex may have a reasonable lifetime during which it may be detected experimentally, but alternatively may be able to act as an oxidant side-by-side with the oxo–iron species. In order to test this hypothesis, further DFT calculations on substrate epoxidation by ^{5}**3** and ^{5}**4** in the catalytic cycle of TauD with respect to a common substrate were performed [42]. In the previous section the reactivity of **4** with respect to propene was discussed in detail and for simplicity the same substrate was used for the studies of the alternative oxidant hypothesis. Thus, **4** reacts with propene with low reaction barriers of 4.8 kcal mol^{-1} to give epoxide product complexes [9]. Fig. 15 gives the potential energy surface starting from the peroxosuccinate complex (**3**) as obtained with DFT calculations. The direct epoxidation barrier is high (24.6 kcal mol^{-1}) and is well higher in energy than the dioxygen cleavage leading to the oxo–iron species. Even the subsequent epoxidation barriers for the oxo–iron complex are well below this dioxygen cleavage barrier so that epoxidation will happen instantaneous as soon as the oxo–iron species is formed. Moreover, the calculations show that the oxo–iron species is the sole oxidant of the TauD enzyme and that its precursor cannot compete in the reactions with substrates. This is in line with DFT and experimental studies on heme model complexes that also showed that the precursor of the oxo–iron species (in that particular case the hydroperoxo–iron complex) is a sluggish oxidant in epoxidation reactions [62].

4. Conclusions

DFT calculations on the catalytic cycles of two dioxygenase enzyme systems (CDO and TauD) have identified short-lived intermediates that are difficult to trap and characterize experimentally or are impossible to stabilize experimentally. The studies have given insight into how oxygen is activated on a nonheme iron center and the factors that stabilize and characterize the reactivity patterns. Important outcomes of the work are that these non-heme dioxygenases appear to be efficient oxidants that react with substrates with small barriers and therefore high reactivity. As such they should be able to catalyze hydroxylation of strong C–H bonds with even better efficiency than the cytochromes P450 for instance. Thus, it may very well be that nature has created two types of oxidants: one group (like the P450s) that are subtle and gentle and able to catalyze regioselective and stereospecific reaction mechanisms whereas the other group (like TauD) contain more aggressive oxidants that hydroxylate almost any C–H bond. Further research to establish the differences and comparisons of heme and non-heme enzyme oxidants is ongoing. Furthermore, the knowledge of enzyme catalysis is being transferred to the synthesis of non-heme biomimetics that can catalyze efficient monoxygenation reactions with high regioselectivity.

Acknowledgement

The National Service of Computational Chemistry Software (NSCCS) is acknowledged for providing the CPU time for the studies presented in this work.

References

[1] (a) E.I. Solomon, T.C. Brunold, M.I. Davis, J.N. Kemsley, S.-K. Lee, N. Lehnert, F. Neese, A.J. Skulan, Y.-S. Yang, J. Zhou, Chem. Rev. 100 (2000) 235;
(b) T.D.H. Bugg, Tetrahedron 59 (2003) 7075;
(c) M. Costas, M.P. Mehn, M.P. Jensen, L. Que Jr., Chem. Rev. 104 (2004) 939.
[2] (a) M. Sono, M.P. Roach, E.D. Coulter, J.H. Dawson, Chem. Rev. 96 (1996) 2841;
(b) W.-D. Woggon, Top. Curr. Chem. 184 (1996) 39;
(c) J.T. Groves, Proc. Natl. Acad. Sci. U.S.A. 100 (2003) 3569;
(d) P.R. Ortiz de Montellano (Ed.), Cytochrome P450: Structure, Mechanism and Biochemistry, 3rd ed., Kluwer Academic/Plenum Publishers, New York, 2004.
[3] (a) F.P. Guengerich, Chem. Res. Toxicol. 14 (2001) 611;
(b) M.J.I. Paine, N.S. Scrutton, A.W. Munro, A. Gutierez, G.C.K. Roberts, C.R. Wolf, Electron Transfer Partners of Cytochrome P450, 2004, p. 115 (in Ref. [2(d)], Chapter 4).
[4] (a) H. Li, S. Narasimhulu, L.M. Havran, J.D. Winkler, T.L. Poulos, J. Am. Chem. Soc. 117 (1995) 6297;
(b) B. Meunier, S.P. de Visser, S. Shaik, Chem. Rev. 104 (2004) 3947;
(c) I.G. Denisov, T.M. Makris, S.G. Sligar, I. Schlichting, Chem. Rev. 105 (2005) 2253.
[5] (a) R. Davydov, T.M. Makris, V. Kofman, D.E. Werst, S.G. Sligar, B.M. Hoffman, J. Am. Chem. Soc. 123 (2001) 1403;
(b) T.S. Dowers, D.A. Rock, D.A. Rock, J.P. Jones, J. Am. Chem. Soc. 126 (2004) 8868.
[6] (a) B.C. Finzel, T.L. Poulos, J. Kraut, J. Biol. Chem. 259 (1984) 13027;
(b) M. Sivaraja, D.B. Goodin, M. Smith, B.M. Hoffman, Science 245 (1989) 738;
(c) G.I. Berglund, G.H. Carlsson, A.T. Smith, H. Szöke, A. Henriksen, J. Hajdu, Nature 417 (2002) 463.
[7] P.J. Riggs-Gelasco, J.C. Price, R.B. Guyer, J.H. Brehm, E.W. Barr, J.M. Bollinger Jr., C. Krebs, J. Am. Chem. Soc. 126 (2004) 8108.
[8] A. Decker, E.I. Solomon, Angew. Chem., Int. Ed. 44 (2005) 2252.

[9] (a) S.P. de Visser, Angew. Chem., Int. Ed. 45 (2006) 1790;
(b) S.P. de Visser, J. Am. Chem. Soc. 128 (2006) 9813.
[10] M.H. Stipanuk, Annu. Rev. Nutr. 24 (2004) 539.
[11] (a) M.J. Ryle, R.P. Hausinger, Curr. Opin. Chem. Biol. 6 (2002) 193;
(b) J.M. Bollinger Jr., J.C. Price, L.M. Hoffart, E.W. Barr, C. Krebs, Eur. J. Inorg. Chem. (2005) 4245;
(c) G.D. Straganz, B. Nidetzky, ChemBioChem. 7 (2006) 1536;
(d) M.M. Abu-Omar, A. Loaiza, N. Hontzeas, Chem. Rev. 105 (2005) 2227.
[12] (a) L.J. Higgins, F. Yan, P. Liu, H.-W. Liu, C.L. Drennan, Nature 437 (2005) 838;
(b) O.W. Choroba, D.H. Williams, J.B. Spencer, J. Am. Chem. Soc. 122 (2000) 5389;
(c) F. Fukumori, R.P. Hausinger, J. Biol. Chem. 268 (1993) 24311.
[13] (a) M.R. Bukowski, K.D. Koehntop, A. Stubna, E.L. Bominaar, J.A. Halfen, E. Münck, W. Nam, L. Que Jr., Science 310 (2005) 1000;
(b) L. Que Jr., Acc. Chem. Res. 40 (2007) 493;
(c) W. Nam, Acc. Chem. Res. 40 (2007) 522.
[14] M.T. Heafield, S. Fearn, G.B. Steventon, R.H. Waring, A.C. Williams, S.G. Sturman, Neurosci. Lett. 110 (1990) 216.
[15] T.L. Perry, M.G. Norman, V.W. Yong, S. Whiting, J.U. Crichton, S. Hansen, S. Kish, J. Ann. Neurol. 18 (1985) 482.
[16] (a) J.G. McCoy, L.J. Bailey, E. Bitto, C.A. Bingman, D.J. Aceti, B.G. Fox, G.N. Phillips Jr., Proc. Natl. Acad. Sci. U.S.A. 103 (2006) 3084;
(b) C.R. Simmons, Q. Liu, Q. Huang, Q. Hao, T.P. Begley, P.A. Karplus, M.H. Stipanuk, J. Biol. Chem. 281 (2006) 18723;
(c) B.D. Pierce, J.D. Gardner, L.J. Bailey, T.C. Brunold, B.G. Fox, Biochemistry 46 (2007) 8569.
[17] S. Aluri, S.P. de Visser, J. Am. Chem. Soc. 129 (2007) 14846.
[18] S. Ye, X. Wu, L. Wei, D. Tang, P. Sun, M. Bartlam, Z. Rao, J. Biol. Chem. 282 (2007) 3391.
[19] J.B. Lombardini, T.P. Singer, P.D. Boyer, J. Biol. Chem. 244 (1969) 1172.
[20] M.T. Green, J. Am. Chem. Soc. 122 (2000) 9495.
[21] E. Godfrey, C.S. Porro, S.P. de Visser, J. Phys. Chem. A 112 (2008) 2464.
[22] (a) R.P. Hausinger, Crit. Rev. Biochem. Mol. Biol. 39 (2004) 21;
(b) C. Krebs, D.G. Fujimori, C.T. Walsh, J.M. Bollinger Jr., Acc. Chem. Res. 40 (2007) 484.
[23] See, for instance:
(a) S.C. Trewick, T.F. Henshaw, R.P. Hausinger, T. Lindahl, B. Sedgwick, Nature 419 (2002) 174;
(b) P.Ø. Falnes, R.F. Johansen, E. Seeberg, Nature 419 (2002) 178;
(c) T. Duncan, S.C. Trewick, P. Koivisto, P.A. Bates, T. Lindahl, B. Sedgwick, Proc. Natl. Acad. Sci. U.S.A. 99 (2002) 16660;
(d) P.A. Aas, M. Otterlei, P.Ø. Falnes, C.B. Vågbø, F. Skorpen, M. Akbari, O. Sundheim, M. Bjørås, G. Slupphaug, E. Seeberg, H.E. Krokan, Nature 421 (2003) 859;
(e) Y. Mishina, E.M. Duguid, C. He, Chem. Rev. 106 (2006) 215.
[24] J.C. Price, E.W. Barr, B. Tirupati, J.M. Bollinger Jr., C. Krebs, Biochemistry 42 (2003) 7497.
[25] J.R. O'Brien, D.J. Schuller, V.S. Yang, B.D. Dillard, W.N. Lanzilotta, Biochemistry 42 (2003) 5547.
[26] L. Que Jr., Nat. Struct. Biol. 7 (2000) 182.
[27] See e.g.;
(a) E.L. Hegg, L. Que Jr., Eur. J. Biochem. 250 (1997) 625;
(b) P.D. Oldenburg, C.-Y. Ke, A. Tipton, A.A. Shteinman, L. Que Jr., Angew. Chem., Int. Ed. 45 (2006) 7975;
(c) P.C.A. Bruijnincx, I.L.C. Buurmans, S. Gosiewska, M.A.H. Moelands, M. Lutz, A.L. Spek, G. van Koten, R.J.M. Klein Gebbink, Chem. Eur. J. 14 (2008) 1228.
[28] (a) S.P. de Visser, S. Shaik, J. Am. Chem. Soc. 125 (2003) 7413;
(b) S.P. de Visser, Chem. Eur. J. 12 (2006) 8168;
(c) A. Ghosh, J. Biol. Inorg. Chem. 11 (2006) 712.
[29] S.P. de Visser, K. Oh, A.-R. Han, W. Nam, Inorg. Chem. 46 (2007) 4632.
[30] (a) J.H. Dawson, R.H. Holm, J.R. Trudell, G. Barth, R.E. Linder, E. Bunnenberg, C. Djerassi, S.C. Tang, J. Am. Chem. Soc. 98 (1976) 3707;
(b) T.L. Poulos, J. Biol. Inorg. Chem. 1 (1996) 356.
[31] (a) P.R. Ortiz de Montellano, Annu. Rev. Pharmacol. Toxicol. 32 (1992) 89;
(b) N.C. Veitch, A.T. Smith, Adv. Inorg. Chem. 51 (2000) 107.
[32] M.J. Ryle, R. Padmakumar, R.P. Hausinger, Biochemistry 38 (1999) 15278.
[33] M.L. Neidig, C.D. Brown, K.M. Light, D.G. Fujimori, E.M. Nolan, J.C. Price, E.W. Barr, J.M. Bollinger Jr., C. Krebs, C.T. Walsh, E.I. Solomon, J. Am. Chem. Soc. 129 (2007) 14224.
[34] D.A. Proshlyakov, T.F. Henshaw, G.R. Monterosso, M.J. Ryle, R.P. Hausinger, J. Am. Chem. Soc. 126 (2004) 1022.
[35] C. Krebs, J.C. Price, J. Baldwin, L. Saleh, M.T. Green, J.M. Bollinger Jr., Inorg. Chem. 44 (2005) 742.
[36] J.C. Price, E.W. Barr, T.E. Glass, C. Krebs, J.M. Bollinger Jr., J. Am. Chem. Soc. 125 (2003) 13008.
[37] J.C. Price, E.W. Barr, L.M. Hoffart, C. Krebs, J.M. Bollinger Jr., Biochemistry 44 (2005) 8138.
[38] P.K. Grzyska, M.J. Ryle, G.R. Monterosso, J. Liu, D.P. Ballou, R.P. Hausinger, Biochemistry 44 (2005) 3845.
[39] J.M. Elkins, M.J. Ryle, I.J. Clifton, J.C. Dunning Hotopp, J.S. Lloyd, N.I. Burzlaff, J.E. Baldwin, R.P. Hausinger, P.L. Roach, Biochemistry 41 (2002) 5185.
[40] M.J. Ryle, K.D. Koehntop, A. Liu, L. Que Jr., R.P. Hausinger, Proc. Natl. Acad. Sci. U.S.A. 100 (2003) 3790.
[41] (a) A. Bassan, T. Borowski, P.E.M. Siegbahn, Dalton Trans. (2004) 3153;
(b) T. Borowski, A. Bassan, P.E.M. Siegbahn, Chem. Eur. J. 10 (2004) 1031.
[42] S.P. de Visser, Chem. Commun. (2007) 171.
[43] (a) A.V. Nemukhin, B.L. Grigorenko, I.A. Topol, S.K. Burt, Int. J. Quant. Chem. 106 (2006) 2184;
(b) A.V. Nemukhin, I.A. Topol, R.E. Cachau, S.K. Burt, Theor. Chem. Acc. 115 (2006) 348;
(c) I.A. Topol, A.V. Nemukhin, K. Salnikow, R.E. Cachau, Y.G. Abashkin, K.S. Kasprzak, S.K. Burt, J. Phys. Chem. A 110 (2006) 4223;
(d) S. Sinnecker, N. Svensen, E.W. Barr, S. Ye, J.M. Bollinger Jr., F. Neese, C. Krebs, J. Am. Chem. Soc. 129 (2007) 6168.
[44] (a) S.P. de Visser, S. Shaik, P.K. Sharma, D. Kumar, W. Thiel, J. Am. Chem. Soc. 125 (2003) 15779;
(b) S.P. de Visser, J. Phys. Chem. A 109 (2005) 11050.
[45] (a) S.P. de Visser, F. Ogliaro, N. Harris, S. Shaik, J. Am. Chem. Soc. 123 (2001) 3037;
(b) S. Shaik, S.P. de Visser, F. Ogliaro, H. Schwarz, D. Schröder, Curr. Opin. Chem. Biol. 6 (2002) 556;
(c) D. Kumar, S.P. de Visser, S. Shaik, Chem. Eur. J. 11 (2005) 2825.
[46] M. Lundberg, K. Morokuma, J. Phys. Chem. B 111 (2007) 9380.
[47] S.P. de Visser, L.M. Mirica, unpublished results.
[48] P. Andreoletti, A. Pernoud, G. Sainz, P. Gouet, H.M. Jouve, Acta Cryst. D 59 (2003) 2163.
[49] (a) S.P. de Visser, F. Ogliaro, P.K. Sharma, S. Shaik, Angew. Chem., Int. Ed. 41 (2002) 1947;
(b) S.P. de Visser, F. Ogliaro, P.K. Sharma, S. Shaik, J. Am. Chem. Soc. 124 (2002) 11809;
(c) D. Kumar, S.P. de Visser, P.K. Sharma, E. Derat, S. Shaik, J. Biol. Inorg. Chem. 10 (2005) 181.
[50] (a) M.T. Green, J. Am. Chem. Soc. 121 (1999) 7939;
(b) S. Shaik, D. Kumar, S.P. de Visser, A. Altun, W. Thiel, Chem. Rev. 105 (2005) 2279.
[51] S.P. de Visser, J. Am. Chem. Soc. 128 (2006) 15809.
[52] (a) S.P. de Visser, J. Biol. Inorg. Chem. 11 (2006) 168;
(b) R. Wang, S.P. de Visser, J. Inorg. Biochem. 101 (2007) 1464;
(c) S.P. de Visser, Inorganic Biochemistry Research Progress, Novascience, New York, 2008;
(d) S.P. de Visser, J. Phys. Chem. B 111 (2007) 12299.
[53] P.K. Sharma, S.P. de Visser, S. Shaik, J. Am. Chem. Soc. 125 (2003) 8698.
[54] D. Kumar, S.P. de Visser, P.K. Sharma, S. Cohen, S. Shaik, J. Am. Chem. Soc. 126 (2004) 1907.
[55] (a) S.P. de Visser, F. Ogliaro, S. Shaik, Angew. Chem., Int. Ed. 40 (2001) 2871;
(b) S.P. de Visser, D. Kumar, S. Shaik, J. Inorg. Biochem. 98 (2004) 1183.
[56] S. Shaik, D. Kumar, S.P. de Visser, J. Am. Chem. Soc. 130 (2008), in press.
[57] S.P. de Visser, D. Kumar, S. Cohen, R. Shacham, S. Shaik, J. Am. Chem. Soc. 126 (2004) 8362.
[58] J.M. Mayer, Acc. Chem. Res. 31 (1998) 441.
[59] J. Kaizer, E.J. Klinker, N.Y. Oh, J.-U. Rohde, W.J. Song, A. Stubna, J. Kim, E. Münck, W. Nam, L. Que Jr., J. Am. Chem. Soc. 126 (2004) 472.
[60] D. Kumar, E. Derat, A.M. Khenkin, R. Neumann, S. Shaik, J. Am. Chem. Soc. 127 (2005) 17712.
[61] S. Shaik, A. Shurki, Angew. Chem., Int. Ed. 38 (1999) 586.
[62] (a) F. Ogliaro, S.P. de Visser, S. Cohen, P.K. Sharma, S. Shaik, J. Am. Chem. Soc. 124 (2002) 2806;
(b) M.J. Park, J. Lee, Y. Suh, J. Kim, W. Nam, J. Am. Chem. Soc. 128 (2006) 2630.